Simulation of a Real-time Local Data Integration System over East-Central Florida

Prepared By:
Applied Meteorology Unit

November 1999

Attributes and Acknowledgments

Table of Contents

List of Figures

List of Tables

List of Acronyms

Term	Description
45 WS	45th Weather Squadron
ACARS	ARINC Communications, Addressing and Reporting System
ADAS	ARPS Data Analysis System
ADDE	Abstract Data Distribution Environment
AMU	Applied Meteorology Unit
ARINC	Aeronautical Radio, Inc.
ARPS	Advanced Regional Prediction System
AMX	Miami, FL 3-letter station identifier
BYX	Key West, FL 3-letter radar site identifier
CAPE	Convective Available Potential Energy
CAPS	Center for Analysis and Prediction of Storms
CC	Correlation Coefficient
CCAS	Cape Canaveral Air Station
CCS	Complex Cloud Scheme
CPU	Central Processing Unit
DNI	Data Non-Incorporation
EOM	End of Mission
FR	Flight Rules
FSL	Forecast Systems Laboratory
GEMPAK	General Meteorological Package
GOES	Geostationary Orbiting Environmental Satellite
HP	Hewlett Packard
IBM	International Business Machine
IR	Infrared
ITWS	Integrated Terminal Weather System
JAX	Jacksonville, FL 3-letter station identifier
KSC	Kennedy Space Center
LAPS	Local Analysis and Prediction System
LCC	Launch Commit Criteria
LDIS	Local Data Integration System
LWO	Launch Weather Officer
MB	Megabyte
McIDAS-X	Man-Computer Interactive Data Access System for UNIX
METAR	Aviation Routine Weather Report

MIDDS	Meteorological Interactive Data Display System
MLB	Melbourne, FL 3-letter station identifier
NEXRAD	Next Generation Radar
NIDS	NEXRAD Information Dissemination Service
NWS	National Weather Service
OI	Optimum Interpolation
PIREPS	Pilot Reports
QC	Quality Control
RH	Relative Humidity
RTLS	Return to Launch Site
RUC	Rapid Update Cycle
SCM	Successive Corrections Method
SLF	Shuttle Landing Facility
SMG	Spaceflight Meteorology Group
TBW	Tampa Bay, FL 3-letter station identifier
TLH	Tallahassee, FL 3-letter station identifier
VIS	Visible satellite imagery
WSR-88D	Weather Surveillance Radar-1988 Doppler
WV	Water Vapor
XMR	Cape Canaveral, FL 3-letter station identifier

This page intentionally left blank.

Executive Summary

The Applied Meteorology Unit (AMU) simulated a real-time configuration of the Local Data Integration System (LDIS) over the Florida peninsula including the Kennedy Space Center (KSC)/Cape Canaveral Air Station (CCAS) using a two-week archived data set from 15-28 February 1999. The task objectives were to assess the utility of a real-time LDIS by simulating a real-time configuration for a period of two-weeks, evaluate and extrapolate system performance to identify the hardware necessary to run LDIS in real-time, and determine the sensitivities and deficiencies of the simulated real-time LDIS configuration and suggest and/or test improvements.

The ultimate goal for running LDIS is to generate products that may enhance weather nowcasts and short-range (< 6 h) forecasts issued in support of the 45th Weather Squadron (45 WS), Spaceflight Meteorology Group (SMG), and Melbourne National Weather Service (NWS MLB) operational requirements. The AMU report entitled Final Report on Prototype Local Data Integration System and Central Florida Data Deficiency (Case and Manobianco 1998, LDIS Phase I) described the fidelity and utility of LDIS for two particular case studies. In this report, the AMU demonstrated that LDIS can provide added value for nowcasts and short-term forecasts because it incorporates all operationally-available data in east-central Florida and it is run at finer spatial and temporal resolutions than current national-scale operational models. The current report (LDIS Phase II) extends these efforts by describing the utility and sensitivities associated with a simulated real-time configuration of LDIS. In a real-time mode, LDIS can provide users with a more comprehensive understanding of evolving fine-scale weather features than could be developed by individually examining the disparate data sources.

The AMU used the same hardware and software as in LDIS Phase I for the simulated real-time configuration. The AMU ran the Advanced Regional Prediction System (ARPS) Data Analysis System (ADAS) software on an IBM RS/6000 workstation to generate high-resolution analyses in space and time. SMG and NWS MLB archived data in real-time and the AMU reconfigured data ingestors for the simulated real-time LDIS based on the data format received at SMG. Rawinsonde, satellite-derived winds, and satellite-derived soundings experience a large real-time latency, and thus the AMU did not ingest these data into ADAS as part of the simulated real-time configuration.

Based on the characteristics of the real-time data ingested into ADAS, the KSC/CCAS wind tower network, KSC/CCAS 915-MHz and 50-MHz wind profilers, and Weather Surveillance Radar-1988 Doppler (WSR-88D) consistently provide the greatest quantity of fine-scale weather observations. Rawinsonde data are generally available every 12 hours, satellite-derived winds every 3 hours, and satellite-derived soundings every hour. The number of available automated and manual aircraft observations vary significantly with time.

The IBM RS/6000 workstation used in this study consists of a 67-MHz single processor with 512 megabytes (MB) of memory. The mean wall-clock time for each ADAS analysis cycle is 7.29 minutes and does not include the time required for data pre-processing or graphical post-processing. In order to obtain analysis products in an operationally useful time frame, SMG specified that the entire analysis cycle, including pre-and post-processing, be completed in about 5 minutes. Based on this specification, the AMU recommends a workstation with at least a 200-MHz single processor and 512 MB of memory for running the LDIS Phase II configuration in real-time. A workstation with less central processing unit speed may be adequate if data pre-processing and graphical post-processing are handled on a separate workstation. Man-Computer Interactive Data Access System for UNIX (McIDAS-X) software version 7.5 or higher is necessary to run the data pre-processing algorithms designed by the AMU.

While simulating a real-time configuration using data archived from 15–28 February 1999, ADAS demonstrated utility in the following weather situations.

- Depicting high-resolution quantitative characteristics of cloud fields such as ceilings, cloud-top heights, cloud liquid content, cloud ice content, etc.

- Monitoring the magnitude of cross, head, and/or tailwind components at the KSC Shuttle Landing Facility (SLF).

- Diagnosing a sea-breeze passage at the SLF.

- Assessing stability indices at high temporal and spatial resolutions to determine thunderstorm risks.

This report presents results for two specific cases from the two-week data archive illustrating the utility of real-time cloud and wind products.

Due to limited bandwidth, SMG cannot receive in real-time the complete volume of WSR-88D data (level II data) directly from the Melbourne, FL radar site. Instead, SMG receives WSR-88D processed data (level III data) from a private vendor. Level III data have fewer vertical scans than level II data, a coarser horizontal resolution compared to level II data, and are categorized into discrete bins, thereby reducing the file sizes substantially. Thus, level III data can be transmitted to SMG in real-time for all Florida radar sites.

The AMU compared analyses ingesting level II versus level III WSR-88D data. In general, the number of available level II radar observations greatly exceeds the number of available level III radar observations. As a result, analyses using level II WSR-88D data can detect more adequately wind shift lines and vertical circulations. However, an advantage of using level III WSR-88D data is that SMG receives data from all Florida radar sites resulting in increased horizontal coverage of radar data at low levels.

The quality and representativeness of the analyzed cloud fields are highly dependent on the available data that are integrated into ADAS. When GOES-8 infrared and visible satellite data are not available, the cloud analysis is often deficient and not able to detect fine-scale cloud features especially when little WSR-88D data are available or there are no targets for the radar to detect. Sharp transitions between successive cloud analyses can occur during sunrise and sunset times due to deficient GOES-8 visible data.

In a real-time configuration, ADAS requires gridded forecasts from a regional-scale numerical prediction model such as the Rapid Update Cycle (RUC) or Eta model as a first-guess field for the gridded analyses. If gridded forecasts are missing then ADAS analyses cannot be generated. Thus, alternative gridded forecast data, such as forecasts from earlier RUC or Eta model runs, must be available as a first-guess field for ADAS analyses in the event that the primary gridded forecast fields are missing.

The AMU conducted data non-incorporation (DNI) experiments for data sources that experience large real-time latencies in order to measure the impact of these data sources on the subsequent analyses. For each DNI experiment, the AMU individually included each data set with all other data and regenerated ADAS analyses for the entire two-week period. DNI results indicate that among the three data sources withheld from the simulated real-time configuration, GOES-8 satellite soundings have the greatest impact on the analyzed patterns of moisture and temperature. Due to the extensive amount of hourly observations in cloud-free regions, GOES-8 satellite soundings can provide the most utility in ADAS analyses compared to other data sources that experience large real-time latencies. Florida rawinsondes influence all analyzed variables but only have a slight impact every 12 hours. GOES-8-derived winds have a small impact on the analyzed wind field every 3 hours.

Currently, AMU efforts are underway to install LDIS as an operational system at SMG and NWS MLB. Additional issues to consider during the installation phase include the software that will be used for post-processing of graphical products, the types of products that will be generated, and the wall-clock time required to run all data ingest algorithms and graphics generation. Finally, the version of the analysis software that will be installed and the hardware platform for running LDIS need to be determined.

1.0   Introduction

The recent development and implementation of many new in-situ and remotely-sensed observations has resulted in a wealth of meteorological data for weather forecasters. In fact, so much data are available that the complexity of short-term forecasts has increased due to the variety and differing characteristics of the multitude of available observations. As a result, the process of integrating these data to prepare a forecast has become more difficult and perhaps too cumbersome. Tools are required to routinely integrate and assimilate data into a single system in order to simplify the analysis and interpretation of the state of the atmosphere while retaining the capabilities of new data sources. Therefore, in the near future, forecasters should anticipate a transition towards analyzing "processed observations" rather than disparate meteorological data (McPherson 1999).

One such system to integrate data has been tested and configured by the Applied Meteorology Unit (AMU) for the Kennedy Space Center/Cape Canaveral Air Station (KSC/CCAS). The Local Data Integration System (LDIS) was configured for east-central Florida and designed to ingest all operationally available data onto a high-resolution analysis grid that can depict mesoscale aspects of clouds and winds over KSC/CCAS. Results from the AMU report entitled Final Report on Prototype Local Data Integration System and Central Florida Data Deficiency (Case and Manobianco 1998, hereafter LDIS Phase I) have shown that much utility can be gained by running a high-resolution mesoscale analysis system.

The current study (LDIS Phase II) extends the LDIS Phase I efforts by describing the utility of a simulated real-time LDIS and examining the sensitivities and deficiencies related to such a configuration. This report provides the Spaceflight Meteorology Group (SMG), the 45th Weather Squadron (45 WS), and the Melbourne National Weather Service (NWS MLB) with information on the utility of a real-time LDIS, the hardware requirements to run LDIS in real-time, the strengths and weaknesses of a real-time LDIS, and additional steps that may be required to implement a real-time LDIS at a particular office.

1.1 Initial Task Objectives

As written in the original task proposal, the objectives for LDIS Phase II were as follows.

- Optimize temporal continuity of the analyses especially for cloud parameters.

- Determine if any modifications are required to run the prototype configuration in real-time on available hardware.

- Simulate real-time LDIS runs using available real-time data for a period of 1-2 weeks.

- Determine the deficiencies and/or sensitivities of the simulated real-time configuration from the additional case studies and suggest and/or test improvements and/or fixes.

Prior to determining the technical details of LDIS Phase II, the AMU explored some preliminary issues regarding the optimization of temporal continuity of the LDIS analyses. Temporal discontinuities occurred as a result of ingesting disparate data sets that are not typically available at each analysis time. This problem was particularly true for the temporal discontinuities in analyzed cloud fields.

Possible remedies to the temporal discontinuity problem were also explored by the AMU. Analyses were generated at more frequent cycles compared to the time interval used in the LDIS phase I study. More frequent analysis cycles resulted in an improved continuity primarily in the wind field. However, it may be necessary to use mesoscale model forecasts that provide high-resolution first-guess fields in order to further improve temporal continuity of analyzed variables, especially cloud fields.

1.2 Modifications to Original Task Plan

The original task objectives were modified slightly based on consensus from a teleconference that took place during January 1999. Because the AMU identified that the primary cause for temporal discontinuities was the presence or absence of various contributing data sources in successive analyses, all customers agreed that little additional time should be spent on improving the temporal continuity of analyzed variables. Instead, the AMU should identify the data types that cause observed discontinuities so that operational forecasters can recognize the influence of specific data sets on LDIS.

It was determined at this teleconference that the AMU should continue using the Advanced Regional Prediction System (ARPS) Data Analysis System (ADAS) software on the same hardware platform as used in LDIS Phase I. The LDIS Phase II task utilized the same hardware and software for two reasons. First, an extensive amount of time would have been required to reinstall ADAS on different hardware or to change analysis software packages. Second, the customers were most interested in determining the hardware necessary to run LDIS in real-time with minimal modifications from the Phase I configuration. Therefore, no modifications to the LDIS Phase I configuration were suggested. Instead, it was decided that the performance of LDIS on the existing hardware will be evaluated and that the AMU will estimate the hardware specifications necessary to run LDIS in real-time.

Based on the results from LDIS Phase I, Weather Surveillance Radar-1988 Doppler (WSR-88D) data contribute significantly toward the analysis of winds and clouds. However, level II WSR-88D data from only the Melbourne site were used in LDIS Phase I whereas level III data are operationally available at SMG for all Florida sites. Level III data consist of reflectivity and radial velocity observations at a slightly degraded horizontal resolution for only the lowest four elevation angles. Therefore, one important issue for the LDIS extension task is to compare the influence of level II versus level III WSR-88D data on the subsequent ADAS analyses. The comparison addresses the impact of using level II versus level III data and the possible benefits in the analyses by using level III data from multiple WSR-88D sites. Section 3.2 discusses the characteristics of level III WSR-88D data whereas the level II/III comparison is presented in Section 6.1.

The updated and final LDIS Phase II task objectives are as follows.

- Simulate a real-time LDIS using available real-time data for a period of 2 weeks.

- Identify the data types that cause observed discontinuities so LDIS users can recognize the data influences.

- Evaluate system performance on existing hardware and extrapolate the performance to determine the hardware necessary to run a real-time LDIS.

- Determine the sensitivities and/or deficiencies of the simulated real-time configuration from additional case studies and suggest and/or test improvements and/or fixes.

The remainder of this report is outlined as follows. Section 2 describes the methodology used to archive real-time data and modify LDIS for a real-time simulation. The characteristics of the real-time data archive are presented in Section 3 whereas the hardware and system performance are described in Section 4. Section 5 provides sample results from the real-time LDIS simulation. The system sensitivities and deficiencies are given in Section 6 and the results from data non-incorporation tests are presented in Section 7. Finally, Section 8 provides a summary and possible future direction towards the implementation of a real-time LDIS.

2.0   Methodology

An appropriate data archiving strategy must be adopted to obtain an optimal two-week data set for the real-time LDIS simulation. Once the optimal data set is selected, several modifications to the data ingestors and LDIS configuration are necessary in order to simulate a real-time configuration. This section describes the data archiving procedures used in this study, outlines the aspects of the LDIS configuration that remained the same as in LDIS Phase I, and addresses the portions of the LDIS configuration that were modified for the real-time simulation.

2.1 Selection of Real-time Data Set

The two-week real-time data archive used in this study is 15-28 February 1999. During a January 1999 teleconference involving the AMU, SMG, 45 WS, and NWS MLB, a methodology was established to select an optimal two-week period in which the AMU could simulate and evaluate the performance of a real-time LDIS configuration. The methodology includes the strategy used to select the optimal data set and data archiving procedures. The methodology for selecting the optimal two-week data set is as follows.

- A continuous data archive was saved for at least a two-week period at both SMG and NWS MLB.

- If an insufficient number of case study days were available due to benign weather during the first two-week time period, then the subsequent two-week period was archived.

- This process began 18 January and persisted until the most suitable two-week data set was archived. A final date (1 April) for the data archiving window was chosen to provide the AMU with sufficient time for running LDIS and analyzing the output, sensitivities, and deficiencies.

The data archiving procedures were performed by the following organizations as follows.

- NWS MLB archived all Melbourne level II WSR-88D data.

- Aeronautical Radio, Inc. (ARINC) Communications, Addressing and Reporting System (ACARS) data were downloaded by the AMU from the Forecasts Systems Laboratory (FSL) web site (http://acweb.fsl.noaa.gov; Schwartz and Benjamin 1995). ACARS data consist of automated aircraft observations of temperature and winds and can provide valuable soundings during aircraft ascents and descents.

- All other data were archived at SMG and sent to the AMU for real-time LDIS simulations. These data were saved directly from their real-time sources and include GOES-8 visible (VIS) and infrared (IR) imagery, level III WSR-88D data for all Florida radar sites, Rapid Update Cycle (RUC) model 0-, 3-, and 6-h forecast grids, and all textual data from the Meteorological Interactive Data Display System (MIDDS).

A significant number of potential case-study days occurred during the last half of February. SMG composed a list of several weather events during this time period (not shown) which could have violated various space shuttle flight rules (FR) if an operation were occurring. Therefore, based on SMG's recommendation, the official data archive for the real-time LDIS simulation was chosen for 15-28 February 1999.

Two days of particular operational interest occurred during this time period. On 19 February, the development of strong low-level west-southwest winds resulted in potential crosswind violations over the Shuttle Landing Facility (SLF). On 28 February, pre-frontal thunderstorms and a cold frontal passage occurred

and included FR and launch commit criteria (LCC) violations for strong winds, low ceilings, precipitation, and thick clouds.

2.2 Unmodified LDIS Configuration

2.2.1 Analysis Software

As in LDIS Phase I, the AMU used the ADAS software available from the Center for Analysis and Prediction of Storms (CAPS) in Norman, OK. ADAS utilizes the Bratseth objective analysis procedure (Bratseth 1986) consisting of a modified iterative successive corrections method (SCM) (Bergthorsson and Doos 1955) that converges to the statistical or optimum interpolation (OI). Bratseth is superior to a traditional SCM because the Bratseth algorithm accounts for variations in data density and observational errors, similar to OI. A pure OI scheme also accounts for dynamical relationships between variables such as wind and pressure, but is computationally more expensive than a SCM. Thus, the Bratseth scheme realizes some advantages of OI while retaining the computational efficiency of a SCM. The LDIS Phase I report provides a more detailed description of the objective analysis algorithm, the complex cloud scheme (CCS), and quality control (QC) procedures associated with ADAS.

ADAS analyzes five variables at each model vertical level: u- and v-wind components, pressure, potential temperature, and RH*. RH* is a moisture variable analogous to dew-point depression and is defined as:

$$\mathrm{RH}^* = \sqrt{1.0 - \mathrm{RH}}, \tag{2.1}$$

where RH is the relative humidity (Brewster 1996). The ARPS/ADAS vertical coordinate is a terrain-following height coordinate analogous to the traditional sigma coordinate.

2.2.2 Nested Grid Configuration

The same nested grid configuration is retained as in LDIS Phase I following the Integrated Terminal Weather System (ITWS; Cole and Wilson 1995). ADAS is run every 15 minutes at 0, 15, 30, and 45 minutes past the hour over outer and inner grids with horizontal resolutions of 10-km and 2-km respectively. The RUC model is used as a background field for the 10-km ADAS analysis and the resulting 10-km analysis is used as a background field for the 2-km analysis. RUC forecasts are received in real-time at SMG interpolated to an 80-km grid with vertical levels every 50 mb from 1000–100 mb. RUC data are linearly interpolated in time every 15 minutes for each 10-km analysis cycle. The 10-km (2-km) analysis grid covers an area of 500 × 500 km (200 × 200 km) and contains 30 vertical levels that extend from near the surface to about 16.5 km above ground level. The terrain-following vertical coordinate is stretched such that the finest resolution (20 m) occurs near the ground whereas the coarsest resolution (~ 1.8 km) occurs at the top of the domain. The horizontal coverage and grid-point distributions for both the 10-km and 2-km analysis grids are shown in Figure 2.1. Counties over east-central Florida are denoted in Figure 2.1b as a reference for discussions in Sections 5 and 6.

2.2.3 Data Ingest Window

The data ingest strategy from LDIS Phase I is retained for the real-time simulation in the current study. Data are ingested at times closest to the valid analysis time within a 15-minute window centered on the analysis time (± 7.5 minutes). In this possible real-time configuration, data ingest would start each cycle after the actual analysis time to allow for the transmission, receipt, and processing of real-time data. This particular strategy is retained for the current study because each analysis cycle consists of observations grouped as closely together in time making the analysis as representative as possible. An alternative data ingest configuration is to start each cycle at the actual analysis time and incorporate all data collected since the previous cycle. However, this data ingest configuration could result in a less representative mesoscale analysis because observational data would be spaced farther apart in time. Moreover, extensive modifications would have been required to update the data ingest programs for this alternative strategy.

Also as in LDIS Phase I, GOES-8 IR and VIS brightness temperature data in an image format are converted/remapped to both the 10-km and 2-km analysis grids every 15 minutes. The brightness temperature data are then used in the CCS of ADAS to derive various cloud fields (see Appendix).
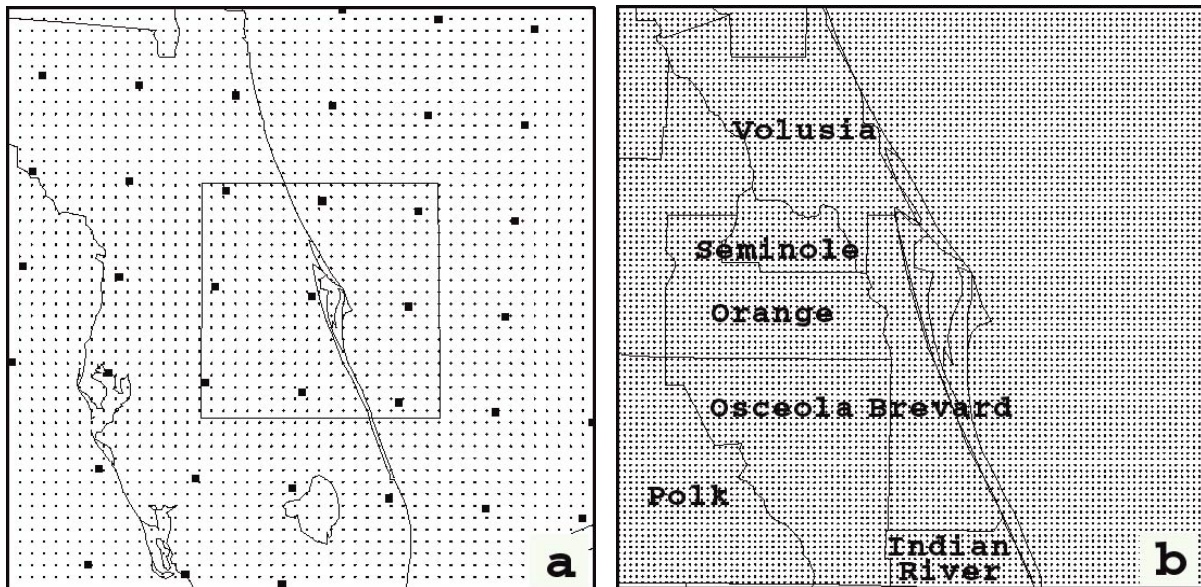
Figure 2.1. The ADAS domains for the 10-km grid and 2-km grid are depicted in panels a) and b), respectively. The 10-km grid point (small dots) and 80-km RUC grid point locations (solid squares) are shown in panel a) while the 2-km grid point locations (small dots) and county labels are shown in panel b). The boxed region in panel a) denotes the 2-km domain.

2.3 Modifications for the Simulated Real-time Configuration

Several modifications to the data ingestors were required in order to appropriately simulate a real-time LDIS configuration. Instead of working with idealized data sets obtained after the fact as in LDIS Phase I, the data archived in real-time are ingested as received into ADAS. Therefore, new issues to address include missing data, data latency between observation and receipt times, and limitations of the available real-time data sets.

2.3.1   Background field

As in LDIS Phase I, the RUC model (Benjamin at al. 1998) is used as a background field for the subsequent 10-km ADAS analyses. However, the RUC data received at SMG have a horizontal resolution of 80 km and a vertical resolution of 50 mb whereas 40-km and 60-km RUC data at 25-mb intervals were used in LDIS Phase I. Furthermore, because the real-time RUC data are received at SMG up to 3 hours after the model initialization time (Table 2.1), RUC 3−6-h forecasts rather than analyses are used as background fields for ADAS.

While converting these RUC data onto the 10-km analysis grid, there are specific times when RUC forecasts are missing from the data archive (not shown). Correspondingly, no ADAS analyses are generated for times when RUC data are not available. This problem could be amended by using older RUC forecast grids (6−12-h forecasts) and/or Eta model forecast grids as a background field for ADAS. However, these options are not feasible in this study because only the RUC 0−6-h forecasts were archived.

Table 2.1.   Real-time data source and estimation of real-time data latency from observation time to receipt time at SMG.

Data Type	Real-Time Source	Time Lag
Surface Observations (METAR)	MIDDS	10 min
Ship/Buoy	MIDDS	10 min
KSC/CCAS Towers	MIDDS	1-2 min
National Rawinsondes	MIDDS	$\geq$ 2.0 h
Cape Canaveral Rawinsonde	MIDDS	20 min
ACARS	NOAA FSL	15 min[1]
PIREPS	MIDDS	5-30 min[2]
GOES-8 VIS/IR	MIDDS	5 min
GOES-8 Soundings	MIDDS	50 min
GOES-8 derived winds	MIDDS	2.0 h
915 MHz profilers	MIDDS	1-2 min
50 MHz profiler	MIDDS	1-2 min
Level II WSR-88D	NWS MLB	< 1 min[3]
Level III WSR-88D	MIDDS	3-5 min
80-km RUC forecast	MIDDS	2.5-3.0 h

[1]Estimated for FSL data.
[2]Estimated for 45 WS MIDDS.
[3]NWS MLB office only (Sharp 1999, personal communication).

2.3.2   Real-time Data

As indicated in Table 2.1, all real-time data sources except ACARS and level II WSR-88D data are available and archived through MIDDS. ADAS reads data in a text format for ingest into the analysis cycle. All the point/textual data available through MIDDS are converted to ASCII format by accessing Man-Computer Interactive Data Access System for UNIX (McIDAS-X) programs non-interactively and preparing the textual data for ingest into ADAS. ACARS data were recently made available in real-time from FSL by means of a local data management feed. Level II WSR-88D data are available in real-time only at NWS MLB.

Due to limitations in their current communication line bandwidth, SMG cannot receive the full-volume level II WSR-88D data in real-time. SMG currently receives level III WSR-88D products in real-time from a NEXRAD (NEXt generation RADar) Information Dissemination Service (NIDS) vendor. The products currently available from SMG's NIDS vendor include reflectivity and radial velocity data for the four lowest elevation angles at the MLB WSR-88D site, and the two lowest elevation angles at all other Florida radar sites (Tallahassee, TLH; Jacksonville, JAX; Tampa Bay, TBW; Miami, AMX; and Key West, BYX). The characteristics of level III WSR-88D products are discussed in more detail in Section 3.

The format of the level III reflectivity and radial velocity products required several modifications to the existing radar conversion/remapping program of ADAS. The existing ADAS remapping program reads WSR-88D level III data from its hybrid coordinates: azimuth, range, and elevation angle. However, the level III products received at SMG are stored on a quasi-horizontal coordinate system (x, y, and elevation angle). Therefore, one of the significant modifications to the remapping program is to identify a common spatial position relative to the WSR-88D radar site. In this instance, latitude, longitude, and height served as the common thread between the two coordinate systems. Once the data positions are identified, the reflectivity and radial velocity data are converted to the analysis grid for ingest into the ADAS algorithms.

The most substantial change in the spatial distribution of the real-time radar data compared to the radar data used in LDIS Phase I is the increased horizontal coverage on the 10-km analysis domain. In LDIS Phase I,

only the MLB WSR-88D data were used and its horizontal coverage is given by the dark shaded region in Figure 2.2a. However, the horizontal coverage of all the radar sites used in LDIS Phase II is denoted by the areas of light and dark shading collectively in Figure 2.2a. The locations of the MLB WSR-88D and the KSC/CCAS data on the 2-km analysis grid are shown in Figure 2.2b.

The MLB WSR-88D influences all of the 2-km domain and a large portion of the 10-km domain (Fig. 2.2a). However, several other Florida radar sites also influence large portions of the 10-km domain (TLH, JAX, TBW, and AMX) and even the 2-km domain (TBW and JAX). Because each level III WSR-88D data set has a range of 230 km, the additive effect of all radar sites results in nearly continuous horizontal coverage of reflectivity and radial velocity data at low-levels on the 10-km and 2-km analysis grids.
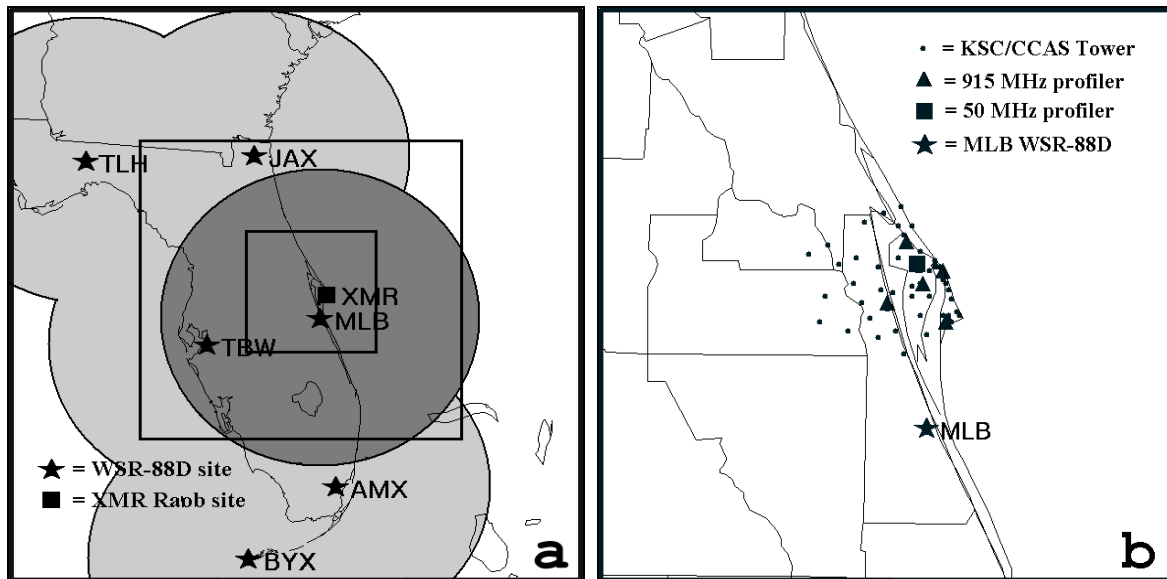
Figure 2.2.   The distribution of WSR-88D data and KSC/CCAS observations in the simulated real-time configuration are shown over the Florida peninsula and the 2-km analysis grids respectively. The dark shading in a) represents the areal coverage of the Melbourne WSR-88D whereas the light and dark shading collectively represent the areal coverage of all Florida radar sites. Outlines of the 10-km (outer) and 2-km (inner) analysis domains and the location of the Cape Canaveral (XMR) rawinsonde also given in a). The locations of the KSC/CCAS towers, 915 MHz and 50 MHz profilers, and the Melbourne WSR-88D are shown in b).

2.3.3   Data Latency

An important issue to consider when configuring LDIS is the lag that occurs between the time of observation and the time that the data are received at a local office. The type and amount of data that should be ingested largely depend on the scales of motion to be sampled and the cycle time of the integration system. Because LDIS is designed to provide mesoscale analyses at 15-minute intervals, the most valuable real-time data sources provide observations at least as often as the analysis cycle. However, if data that experience large time lags are ingested into ADAS, then outdated information could be incorporated — especially during rapidly-evolving mesoscale weather such as deep convection and outflow boundaries.

Table 2.1 provides a summary of the estimated time lags for each real-time data source as received locally at SMG (Oram 1999, personal communication). The AMU identified three data sources with substantial time lags and excluded these data from the real-time LDIS simulation based on several considerations.

- According to the time lags in the third column of Table 2.1, national rawinsondes (2 h), GOES-8 derived winds (2 h), and GOES-8 soundings (50 min) experience time lags significantly longer than the cycle time for LDIS (15 min).

- ADAS does not currently have the capability to time-weight observational data as in the data assimilation systems currently used in the national-scale operational models (such as the RUC and Eta).

- Other analysis systems run in an operational configuration have withheld data with large time lags. For instance, the Local Analysis and Prediction System (LAPS) was run operationally to provide weather support for the 1996 summer Olympic games. LAPS generated surface (upper-air) analyses every 15 (30) minutes across the southeastern United States at a horizontal resolution of 8 km. In the LAPS real-time configuration, data with large time lags such as rawinsondes were not ingested (Snook et al. 1998).

- National rawinsondes and GOES-8 derived winds are currently ingested into the RUC hourly data assimilation cycle (Benjamin and Brundage 1999). Therefore, these two data sources already have an indirect impact on the ADAS analyses through the RUC background fields.

The real-time LDIS simulation excluding national rawinsondes, GOES-8 derived winds, and GOES-8 soundings is referred to as the control simulation. The LDIS control simulation is used for the real-time benchmark and for comparison purposes in data non-incorporation experiments discussed in Section 7. In the data non-incorporation experiments, LDIS is rerun by individually including each of the three data sets with large latency and comparing these new analyses to the control simulation.

2.3.4   Multi-pass Configuration

This section describes in detail some of the tuning parameters of the Bratseth objective analysis scheme as used in ADAS and the modifications made for the real-time configuration. In addition to realizing the advantages of an OI scheme, a multi-pass Bratseth scheme analyzes observational data in separate iterations, or passes, such as the SCM method. Observational data with similar spatial resolutions and sampling characteristics are analyzed together in the same computational pass. This partition ensures that the analyses preserve the resolvable meteorological features of each data source. ADAS tunable parameters are determined based on the characteristics of the observational data that are analyzed in a specific pass.

ADAS uses tunable horizontal and vertical range parameters that determine the influence of observational data within the analysis domain. At larger (smaller) distances from a grid point, observations receive less (more) weight according to a Gaussian-like function. The horizontal and vertical influence ranges, L_h and L_v, are carefully chosen for each data source in order to retain resolvable observational features and to prevent data from influencing too much (or too little) of the analysis grid. Data with a fine (coarse) horizontal resolution are assigned a small (large) L_h to preserve the resolvable features of the data source. In addition, a small L_v is used for data with fine vertical resolution (e.g. KSC/CCAS profilers and towers) and for data that should have a limited vertical influence (e.g. surface observations). Both L_h and L_v are expressed in height coordinates and fixed for all analyses.

As a result of the exclusion of the three data sources discussed in Section 2.3.3, some minor modifications are made to the multi-pass configuration for ADAS as compared to LDIS Phase I. The tunable parameters and data used on each pass are given in Table 2.2. Four computational passes are used for both the 10-km and 2-km ADAS analyses and the same data sets are analyzed in the same passes for both grids. It is important to mention that only the Cape Canaveral (XMR) rawinsonde is used in the real-time configuration instead of all Florida rawinsonde observations as in LDIS Phase I. Also note that the horizontal range parameters L_h have a 5:1 ratio between the 10-km to 2-km values which is the ratio of the horizontal resolution of the 10-km to 2-km grids.

Table 2.2. A list of the objective analysis parameters for the real-time ADAS simulation consisting of the horizontal (L_h; km) and vertical correlation ranges (L_v; m) and data usage for each pass for both the 10-km and 2-km grids.

Pass #	10 km Analysis			2 km Analysis		
	L_h (km)	L_v (m)	Data Used	L_h (km)	L_v (m)	Data Used
1	150	250	Air, Raob	30	250	Air, Raob
2	100	20	Sfc	20	20	Sfc
3	50	20	Tower, Prof	10	20	Tower, Prof
4	20	100	Radar	4	100	Radar

Air = ACARS + Pilot reports (PIREPS)
Sfc = METAR + buoy/ship
Tower = KSC/CCAS towers
Radar = Level III WSR-88D products for all Florida radar sites (Jacksonville, Key West, Miami, Melbourne, Tallahassee, Tampa)
Prof = 915 MHz and 50 MHz KSC/CCAS profilers
Raob = Rawinsonde for XMR only

2.4 Graphical Post-Processing

A series of graphical products are routinely generated with each ADAS analysis cycle in order to qualitatively determine the utility of a real-time LDIS. The 10-km and 2-km ADAS analysis files are converted to General Meteorological Package (GEMPAK) formatted files that are used to create various graphics. Visual products are generated to emphasize clouds, winds, and other fields that would be operationally useful. Among the products created every 15-minutes include horizontal and vertical slices of wind speed and direction, divergence, vertical velocity, cloud liquid and ice mixing ratios, precipitation mixing ratios, relative humidity, cloud ceilings, cloud fractions, and cloud-top heights. Convective parameters and surface temperature plots are generated every hour while time-height cross sections are produced every six hours for analyzed cloud, wind, and moisture variables.

As a possible real-time configuration, the graphical products are created on a separate workstation than the platform used for the ADAS analysis programs. By running the graphical routines on a separate workstation, the total wall clock time for each analysis cycle was reduced dramatically compared to running ADAS and GEMPAK routines on the same machine. Section 4 will discuss in more detail the issues related to system performance and wall clock times for the ADAS analysis and GEMPAK conversion programs.

2.5 Summary of LDIS Configuration Modifications

Table 2.3 provides a summary of the analysis configuration in LDIS Phase I versus Phase II. The primary configuration changes for the real-time simulations include the following.

- Use of 80-km RUC 3−6-h forecasts as background fields for the 10-km ADAS analysis.

- Exclusion of data sources with large time lags compared to the analysis cycle (Florida rawinsonde sites except the Cape Canaveral site, GOES-8 derived winds, and GOES-8 soundings).

- Use of level III WSR-88D data from all Florida radar sites.

Table 2.3. Comparison between the analysis configuration in LDIS Phase I versus Phase II.		
Configuration	**LDIS Phase I**	**LDIS Phase II**
Software	ADAS	ADAS
Hardware	IBM RS/6000	IBM RS/6000; HP (graphics)
Grid	10-km, 2-km nest	10-km, 2-km nest
Cycle frequency	Every 15 minutes on 1/4 hour	Every 15 minutes on 1/4 hour
Data ingest	± 7.5 minutes	± 7.5 minutes
Background field	40-km, 60-km RUC 0-h forecasts	80-km RUC 3−6-h forecasts
Point/Text data	Ingests all data sources	Excludes data with large time lags
Satellite data	GOES-8 IR/VIS	GOES-8 IR/VIS
WSR-88D data	Level II, MLB only	Level III, all FL sites

3.0   Characteristics of the Real-time Data Set

This section provides a description of the data characteristics for the 15-28 February data archive. The average numbers of observations ingested into ADAS are computed at each 15-minute analysis time for nine different data sources (ACARS, GOES-8 derived winds, PIREPS, rawinsondes for XMR only, surface observations, KSC/CCAS towers, GOES-8 satellite soundings, KSC/CCAS profilers, and remapped WSR-88D data). A single observation is considered as a distinct measurement at a particular horizontal location and height. Thus, multiple observations are available at a single time from instrumentation that provides multi-level measurements such as profilers and soundings. A detailed description of level III WSR-88D data is also provided along with some comparisons between the characteristics of level II versus level III WSR-88D data.

3.1 Temporal Distribution of Data

To illustrate the temporal distribution of data ingested into ADAS, the mean number of observations is computed for every 15-minute analysis time for 15-28 February. The sample size is relatively small ($\leq$ 14 days for each time depending on missing observational and/or RUC data); however, the average number of observations given as a function of time helps to show the data dense versus sparse times for each data source.

Surface METAR observations, the XMR rawinsonde, and satellite-derived winds are grouped together as synoptic observations. As expected, the mean number of surface observations in the 10-km analysis domain peaks at the top of every hour with values generally between 30 and 35 (Fig. 3.1a). Special METAR observations contribute to the off-hourly numbers at generally less than 5 per analysis cycle. Satellite-derived wind observations (not used in the LDIS control simulation) are few in number on the 10-km domain. These observations are available every 3 hours at 0145, 0445, 0745, 1045, 1345, 1645, 1945, and 2245 UTC.

A problem occurred in the archiving procedures at SMG and satellite-derived winds were not available at 2245 UTC. At all other available times, satellite-derived winds number less than 25 on average in the 10-km domain. The XMR rawinsonde observations are converted to discrete single-level observations using the same method as described in the LDIS Phase I report. As anticipated, XMR rawinsonde observations peak at 0000 UTC and 1200 UTC, however, some observations were taken between 1600 UTC and 2300 UTC (Fig. 3.1a). These special rawinsonde observations occurred in support of a mission on 15 February.

The mean number of aircraft observations consisting of ACARS and PIREPS display an irregular distribution through all analysis times. The peaks in the mean number of observations occur at random times throughout the entire 24-hour time period (Fig. 3.1b). However, one distinction to note is that both ACARS and PIREPS generally peak at the same times (i.e. 0130, 0300, 0500, 1130, 1215, 1600, 1800, 1930, 2230, and 2330 UTC). The primary exception to this trend occurs at 1030 UTC when ACARS has a distinct maximum in the average number of observations whereas PIREPS has virtually no observations at this time.

The local observations (KSC/CCAS towers and profilers) are the most reliable data source in delivering a relatively uniform number of observations at every analysis time. The tower observations are especially consistent providing a mean number of observations between 100 and 120 for most analysis times on the 10-km analysis grid (Fig. 3.1c). Profiler data tend to vary slightly more than tower data due to QC or data non-receipt. Typically, the mean values in Figure 3.1c vary only because data were missing from the archive at certain times.

The GOES-8 satellite soundings (not used in the LDIS control simulation) and WSR-88D radial velocity observations for all six Florida sites on the 10-km domain are shown in Figure 3.1d. GOES-8 satellite soundings provide 100-175 vertical profiles of temperature and moisture across the 10-km domain during cloud-free conditions. Each GOES-8 profile contains about 40 vertical levels, of which 20 levels are typically within the vertical extent of the analysis domain (surface$-$16.5 km). As a result, between 2000 and 3500 GOES-8 sounding observations occur on the 10-km domain every hour at 15 minutes past the hour (Fig. 3.1d). The number of WSR-88D remapped radial velocity observations are quite consistent on average with values on the order of a few hundred observations for nearly all analysis times. Based on the distribution of the mean

number of observations on the 10-km domain in Figure 3.1, the local KSC/CCAS data and WSR-88D data provide the most consistent and greatest number of mesoscale observations at each analysis time.

Figure 3.1.   The mean number of observations in the 10-km domain for each 15-minute analysis time are given for the following data sources: a) GOES satellite-derived winds (SWN), rawinsondes (RAO), and surface METAR, ship, and buoy observations (SFC), b) ACARS (ACR) and PIREPS (PRP), c) KSC/CCAS towers (TWR) and 50 MHz and 915 MHz profilers (PRO), and d) WSR-88D (RADAR) and GOES-8 satellite soundings (SAT).

Figure 3.2 shows the same plots of mean observational data as in Figure 3.1, except for the 2-km analysis domain. With the exception of XMR rawinsonde observations (Fig. 3.2a), KSC/CCAS data (Fig. 3.2c), and WSR-88D data (Fig. 3.2d), all other observations experience a decrease in the mean number because of the decrease in areal coverage of the 2-km analysis domain. The XMR rawinsonde and KSC/CCAS data contain the same number of observations as in the 10-km analysis domain because these observations lie entirely within the nested 2-km domain.

It is important to note the substantial increase in the number of WSR-88D radial velocity observations on the 2-km domain (Fig. 3.2d) as compared to the 10-km domain (Fig. 3.1d). Whereas the 10-km domain has a few hundred data points on average, the 2-km domain contains from several hundred to 2000 observations. Radar data are remapped onto grid points by averaging all data points that fall in each grid volume. A grid volume for a given grid point has the dimensions of dx × dy × dz, where dx and dy are equal to the horizontal resolution and dz is the vertical resolution. Two aspects of the WSR-88D remapping algorithm influence the number of remapped radial velocity and reflectivity observations on the analysis grids (Brewster 1996). First, a minimum percentage of data coverage in each grid volume is required to generate a legitimate average value for that grid volume. Second, data are rejected for grid volumes that contain a high degree of variance among the data points. Because the individual grid volumes are much smaller in the 2-km rather than 10-km analysis grid, the percentage coverage per grid volume is larger and the variance within each grid volume is smaller. Therefore, more radial velocity and reflectivity data are remapped to the 2-km grid compared to the 10-km grid.
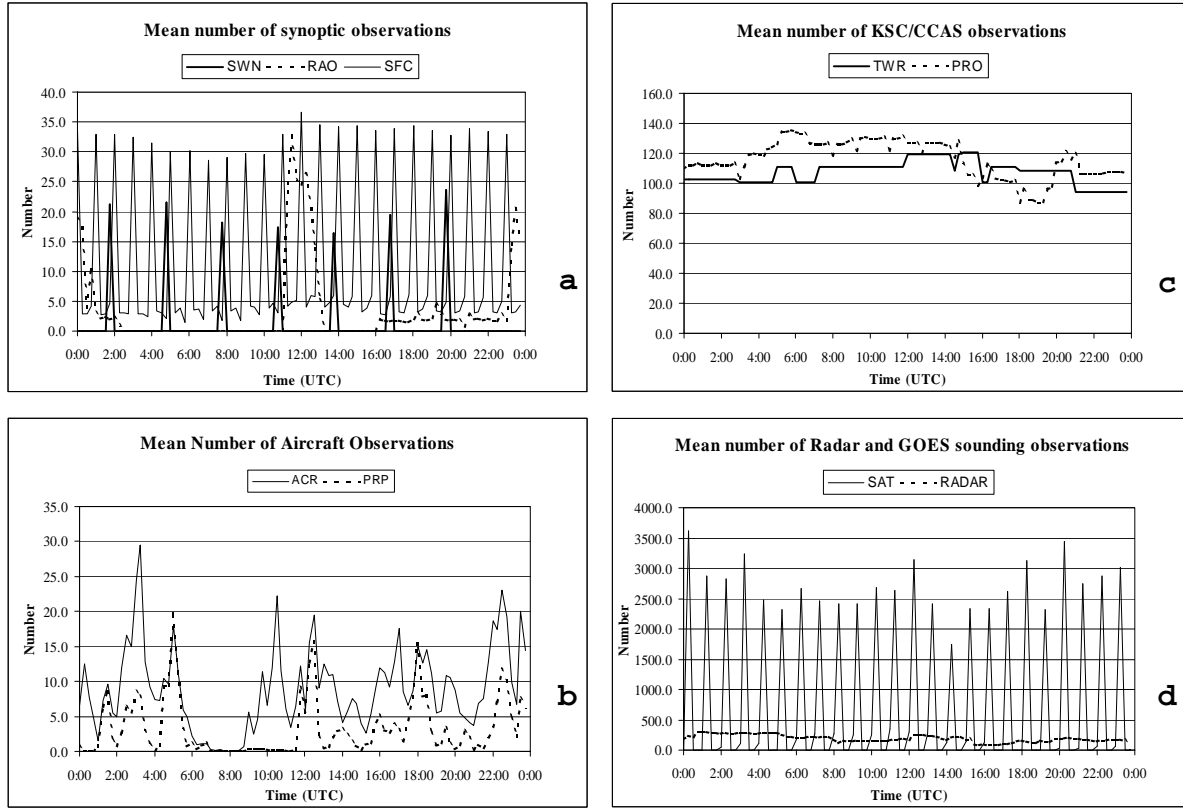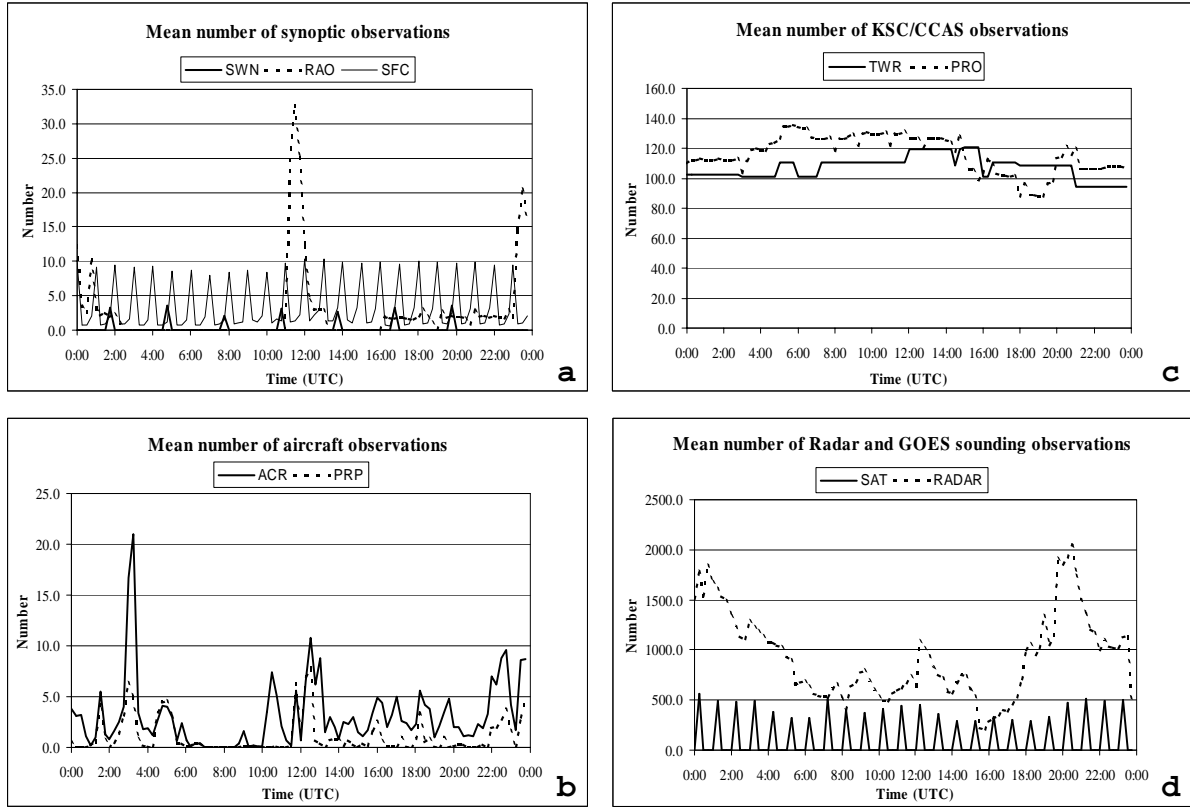
Figure 3.2. The mean number of observations in the 2-km domain for each 15-minute analysis time are given for the following data sources: a) GOES satellite-derived winds (SWN), rawinsondes (RAO), and surface METAR, ship, and buoy observations (SFC), b) ACARS (ACR) and PIREPS (PRP), c) KSC/CCAS towers (TWR) and 50 MHz and 915 MHz profilers (PRO), and d) WSR-88D (RADAR) and GOES-8 satellite soundings (SAT).

3.2 Level III WSR-88D Data

Level III WSR-88D data provide national coverage of real-time radar data through a suite of derived products. These products are provided by NIDS vendors and require a smaller bandwidth for transmission than real-time level II data. Thus, many agencies resort to level III products in order to examine real-time data from multiple radar sites. This section explores the characteristics of the level III WSR-88D products as received at SMG.

Several types of radar products are available in the level III format. However, these products have limitations compared to the full-resolution level II WSR-88D data. Some of the available products include reflectivity, radial velocity, composite reflectivity, vertically integrated liquid, accumulated surface rainfall, and velocity azimuth display winds. Only the lowest four elevation angles of reflectivity and radial velocity data are available in level III WSR-88D data as opposed to fourteen elevation angles with level II data using volume coverage pattern 11. The horizontal resolution is slightly degraded in level III data, on the order of 1 km compared to 250 m gate-to-gate resolution in level II data. The temporal frequency of level III data is the same as level II data.

For the LDIS Phase II study and future operational use, SMG arranged to receive real-time level III data for all Florida radar sites (TLH, JAX, TBW, MLB, AMX, and BYX). However, SMG receives all four elevation angles of level III reflectivity and radial velocity data for the MLB site only. SMG receives the lowest two elevation angles for all other Florida radar sites (Fig. 3.3).

Another limitation of level III WSR-88D data is that reflectivity and radial velocity data are grouped into discrete bins consisting of assigned numerical values. As a result, the numerical values of reflectivity and radial velocity from level II data are rounded to the nearest assigned bin value. These rounding errors can lead to unrepresentative reflectivity and especially radial velocity information (up to 7 m s^{-1} errors in certain cases). The categorized values of reflectivity and radial velocity for both precipitation and clear air modes are given in Table 3.1.

Only the reflectivity and radial velocity products are used by ADAS to build analyses of winds, clouds, and moisture. Reflectivity data are used to build the moisture and cloud analysis fields whereas radial velocity data are utilized for the analyzed wind field. In LDIS Phase I, it was found that level II WSR-88D data contributed strongly to the moisture and wind analyses. Therefore, it is important to compare the influence of level II versus level III WSR-88D on the subsequent analyses. This comparison is performed in Section 6 for a several hour period on 28 February.

Table 3.1. Categorization of level III reflectivity and radial velocity product data into assigned bins.		
Mode	**Reflectivity**	**Radial Velocity**
Precipitation	16 levels: 0–75 dBZ, every 5 dBZ; 1 missing data level	16 levels: -64,-50,-36,-26,-16,-10, -1,0,10,16,26,36,50,64 kts; 1 missing data level; 1 range folding.
Clear Air	16 levels: -28 to +28 dBZ, every 4 dBZ; 1 missing data level	Same as above
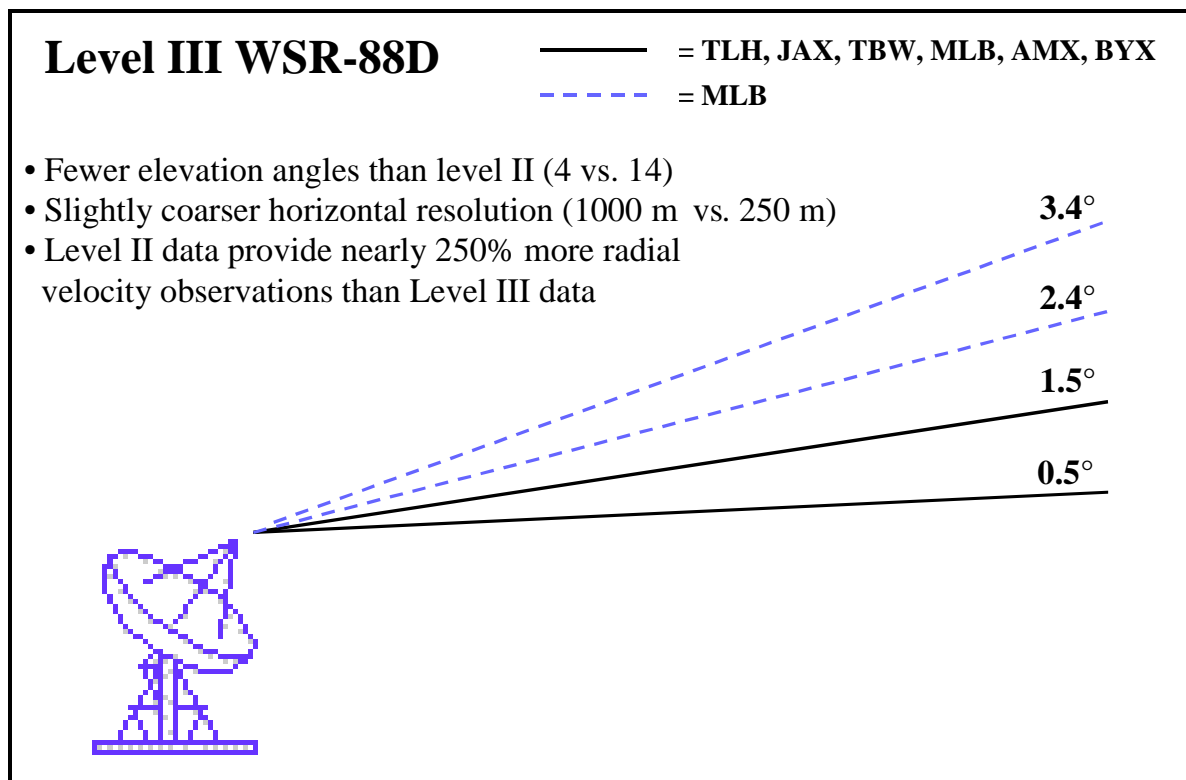
Figure 3.3. A picture is provided showing an illustration and listing of the general characteristics of the real-time level III WSR-88D data configuration at SMG. The Melbourne (MLB) radar site contains data for the four lowest elevation angles whereas Tallahassee (TLH), Jacksonville (JAX), Tampa (TBW), Miami (AMX),

and Key West (BYX) provide data for only the lowest two elevation angles at SMG. The AMU used these available radar data from SMG for ingest into ADAS.

4.0   Hardware and System Performance

In this section, some fundamental hardware characteristics are presented for the AMU workstation used to simulate the real-time LDIS runs. The system performance is documented for the two-week simulation and the real-time requirements for SMG are discussed. Some estimated hardware characteristics are proposed for a workstation necessary to run LDIS in real-time.

4.1 Hardware used

The AMU ran the ADAS analysis cycle on an IBM RS/6000, machine type 7012, model 390 workstation. This workstation contains a 67-MHz processor and a PWR2 chip. Allocated memory is maximized on this machine at 512 megabytes (MB) whereas the standard memory with this workstation is only 32 MB. The 512 MB of memory is necessary to run ADAS because the 2-km analysis program is run on a 100x100x30 grid and requires 267 MB of memory. All other ADAS programs within the analysis cycle require less memory.

For post-processing, the AMU ran various GEMPAK programs to generate graphical display products for qualitative examination. In order to complete the two-week simulation in a reasonable time frame, all graphics were generated on a separate HP workstation in conjunction with the ADAS analysis cycle on the IBM machine. However, since specific graphical products are so highly dependent on the operational needs of each individual office, the run-time performance of the graphical programs are not discussed in this report.

4.2 Run-time Performance

All programs involved in the ADAS analysis cycle and their corresponding wall-clock times are given in Table 4.1. The ADAS cycle is composed of several programs for creating the analyses, interpolation, and conversion to GEMPAK format. First, RUC variables on pressure coordinates are interpolated to the ADAS 10-km grid. The 10-km ADAS analysis is then performed and the resulting data are converted to GEMPAK format for post-processing. The 10-km ADAS cloud products (cloud-top heights, ceilings, and cloud fraction) are also converted to GEMPAK format. Another conversion program interpolates the 10-km analysis data to the 2-km ADAS grid. Following this interpolation, the 2-km analysis is performed followed by a conversion to GEMPAK format. Finally, the 2-km cloud analysis products are converted to GEMPAK format.

The mean wall-clock time of each program in the ADAS cycle indicates that the current analysis configuration runs in real-time on the AMU's IBM RS/6000 workstation. The ADAS analysis cycle averages 7.29 min for all cycles in the two-week simulation period (Table 4.1). Given that the analysis cycle completes every 15 minutes, the current configuration on the AMU workstation runs faster than real-time, but does not include data pre-processing and graphical post-processing times.

Table 4.1.   The mean and standard deviations of wall clock run-times for each program in the ADAS analysis cycle are given along with the total cycle time. These times are valid for the IBM RS/6000 UNIX workstation in the AMU lab and do not include data ingest, conversion, and post-processing times for graphics production.

ADAS Program	Mean Wall Clock Time (min)	Standard Deviation (min)
RUC to 10-km grid conversion	0.48	0.04
10-km ADAS	1.28	0.07
10-km to 2-km grid conversion	2.20	0.38
2-km ADAS	3.33	0.64
Total Wall Clock Time	7.29	----

4.3 Estimation of Hardware Required for Real-time

In an operational mode, the 7.29-minute cycle wall-clock time on the AMU workstation is not sufficient because data preparation, analysis computations, and graphical post-processing should all be completed within about 5 minutes of the analysis window according to SMG specifications. SMG determined this 5-minute constraint based on the need to obtain operational analysis products in a timely fashion. This constraint requires a workstation that can complete the analysis cycle approximately three times faster than the IBM RS/6000 machine used in this study. Because all facets of computer hardware have improved over the past several years since the AMU acquired the IBM RS/6000 machine, it is difficult to address the exact specifications required to run the ADAS cycle in a given amount of time. Besides increasing the central processing unit (CPU) speed, several other factors will also reduce the wall-clock time including improved input/output capabilities with new hard disk drives and improved network connections. These factors and others beyond the scope of this report can influence the wall-clock times for individual ADAS programs.

By focusing on just the CPU speed and no other factors, a workstation with at least a 200-MHz processor should be sufficient to run the ADAS cycle about three times faster than the IBM workstation used in this study. Furthermore, increased efficiency can be obtained by utilizing a workstation with multiple processors. For example, a two-processor workstation at 200-MHz CPU speed per processor would run faster than a single processor workstation with the same CPU rating. Also, the maximum memory used by any of the ADAS programs is 267 MB. Therefore, the memory of the workstation must exceed 267 MB and the AMU suggests at least 512 MB of memory on a workstation used for a real-time LDIS. It should be noted that the AMU will receive a new IBM workstation with two processors, each at 200 MHz CPU speed. The new workstation will contain 1024 MB of memory for advanced visualization capabilities. It is anticipated that this workstation will accommodate SMG's wall-clock specifications for running LDIS in real-time. Future testing could be performed on this new workstation for LDIS Phase III to obtain some approximate wall-clock times for this particular workstation.

Two other aspects of the real-time LDIS are the preparation of all data sources for ingestion into ADAS and the post-processing of graphical analysis products. A good strategy for data preparation could be to run all data converters on a separate workstation connected to the same network as the LDIS workstation. In this study, most of the real-time point and text data are prepared for ADAS using McIDAS-X programs (version 7.501). Therefore, the pre-processing workstation must accommodate McIDAS-X version 7.5 or higher which utilizes the Abstract Data Distribution Environment (ADDE) format. GOES-8 imagery and WSR-88D data are remapped onto the analysis grids and therefore require extra wall-clock time in addition to the ADAS analysis cycle (not shown). In general, the wall-clock times for data ingestion are relatively negligible compared to the actual analysis and interpolation programs. If the workstation used for a real-time LDIS has a sufficiently fast processor speed, then it could be used for running the data ingestors, the ADAS analysis cycle, and graphical post-processing. However, the data ingestors and graphical post-processing could also be run on a separate workstation whereas the LDIS workstation is dedicated to the analysis cycle given in Table 4.1. By running on two separate workstations, the machine dedicated to the ADAS cycle will not require such a fast processor, and thus will not be as expensive.

5.0 Sample Results

In this section, graphical results from the real-time LDIS simulation are presented for two particular cases from the 15−28 February archive. The first case involves strong west-southwest crosswinds in the vicinity of the SLF from 19 February 1999. The space shuttle orbiter is constrained to a 7.7-m s^{-1} (15-kts) peak crosswind component for an end of mission (EOM) or return to launch site (RTLS) landing at the SLF during the daylight hours according to established orbiter FR (Brody et al. 1997). Other peak crosswind constraints include 6.2 m s^{-1} (12 kts) for an EOM or RTLS landing during the night and 5.2 m s^{-1} (10 kts) for an EOM landing in the event of an auxiliary power unit failure. All of these peak crosswind constraints apply to the 9.1-m (30-ft) observation level at the SLF KSC/CCAS tower. Sustained wind products are shown for this particular day and illustrate how LDIS can depict the development and evolution of strong crosswinds at the SLF.

The second case consists of a pre-frontal line of thunderstorms and an accompanying cold frontal passage from 28 February. Lightning, thick cloud, and ceiling rules were all violated within the context of the LCC and orbiter FR on this particular day. The derived cloud-top and ceiling heights are shown in order to illustrate the value of using LDIS in real-time to quantitatively diagnose cloud properties associated with the convective line.

5.1 19 February 1999 (strong crosswinds at the SLF)

This day was characterized by a well-mixed environment ahead of a frontal zone to the north. Surface winds were initially light out of the southwest prior to 1400 UTC but as the mixed layer deepened, the winds shifted to west-southwesterly and increased in magnitude across east-central Florida. According to KSC/CCAS tower observations, peak wind speeds reached ~ 12 m s^{-1} (23 kts) at the 16.5-m level and ~ 13 m s^{-1} (25 kts) at 49 m and 62 m by 1830 UTC (not shown). At the 9.1-m (30-ft) level, the peak crosswind reached 8.7 m s^{-1} (17 kts) at 1715 UTC which violated the 7.7 m s^{-1} (15-kts) crosswind limit for landing at the SLF.

The utility of a real-time LDIS in this situation becomes apparent when examining hourly plots of the LDIS-derived sustained winds in Figure 5.1. The LDIS sustained winds can be used to estimate the actual peak winds recorded at the SLF 9.1-m (30-ft) towers. The hourly plots range from 1400 UTC to 1900 UTC and illustrate the steady increase in the west-southwest winds with time at the 10-m (32.8-ft) analysis level. In the event of an EOM or RTLS landing on this day, the orbiter would have been constrained to a 7.7-m s^{-1} (15-kts) peak crosswind (from a west-southwest direction) at the 9.1-m (30-ft) level. Each panel of Figure 5.1 denotes all three FR thresholds for crosswinds at the SLF (10, 12, and 15 kts) through varying degrees of shading.

Between 1400 and 1500 UTC, LDIS-derived sustained winds are generally south-southwesterly across the domain at speeds less than 5 m s^{-1} (Figs. 5.1a and b). A shift to a more westerly component occurs by 1600 UTC (Fig. 5.1c) as the speed increases to > 5 m s^{-1} across much of the 2-km analysis grid. Speeds continue to increase through 1700 UTC and 1800 UTC as the direction becomes uniformly west-southwest (Figs. 5.1d and e). Finally, by 1900 UTC, sustained crosswind violations, as depicted by gray shading, occur across all of east-central Florida to varying degrees, however, only the 5.2−m s^{-1} (10-kts) criterion is violated over the SLF at this time. These displays of wind speeds and wind vectors that highlight various FR criteria can provide a good estimate of the sustained and peak winds normal to the runway at the SLF.

The development and evolution of the relatively strong sustained crosswinds are depicted by a sequence of low-level west-east cross sections in Figure 5.2. At 1400 UTC, a strong vertical gradient in wind speed exists in the lowest 1000 m ranging from 4 m s^{-1} near the ground to over 13 m s^{-1} at 1000 m (Fig. 5.2a). By 1500 UTC, wind speeds increase to 5.2 m s^{-1} at the lowest analysis level as shown by the shading in Figure 5.2b. At 1600 UTC, the stronger winds aloft continue to mix downward (Fig. 5.2c) resulting in a wind shift to southwest at 10 m (Fig. 5.1c). The 10-m winds continue to veer over the next 2 hours (Figs. 5.1d-e) as the low-level wind speeds steadily increase (Fig. 5.2d-e). By 1900 UTC, sustained wind speeds exceed 7.7 m s^{-1} (15 kts) throughout the depth of the cross section (Fig. 5.2e).
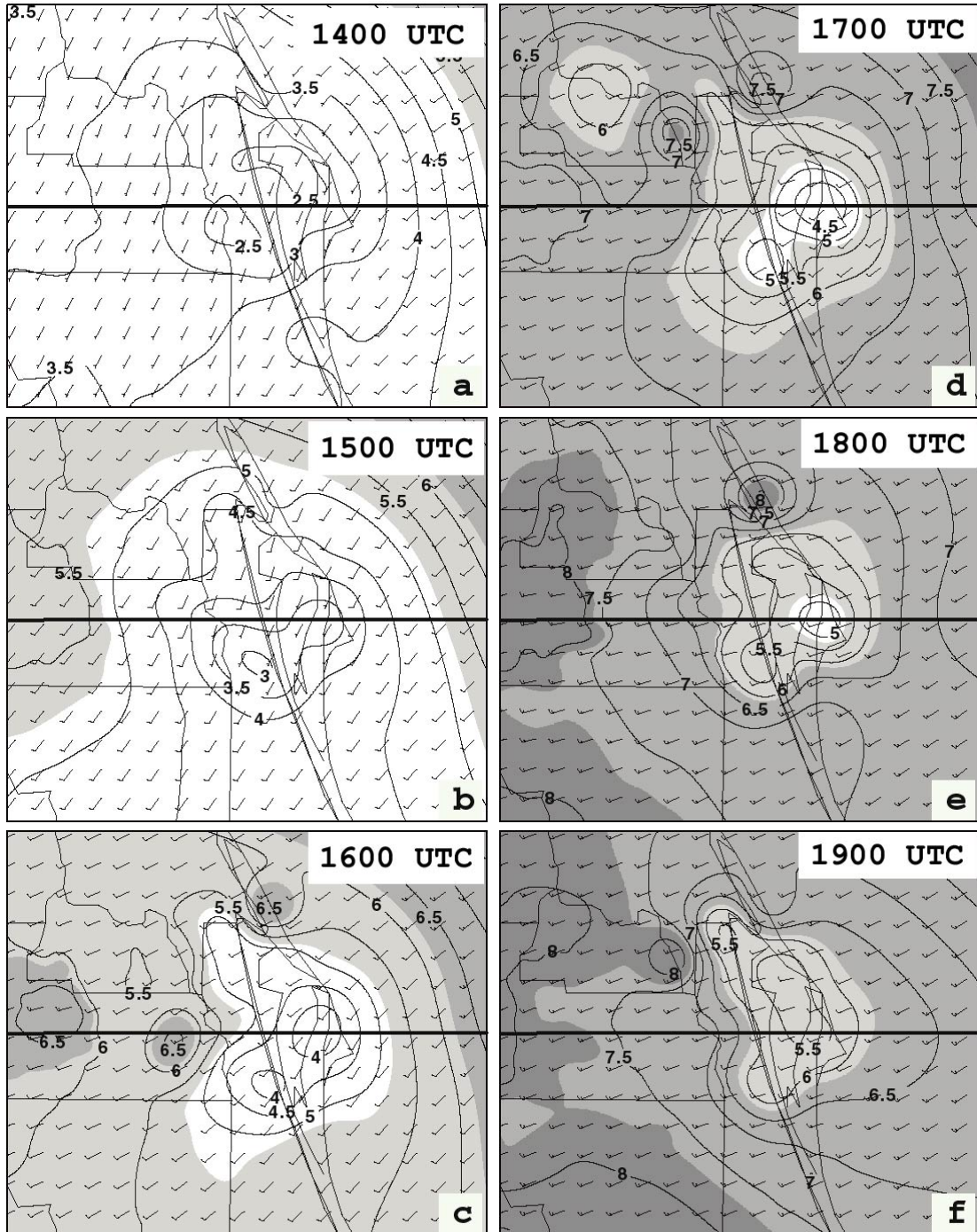
Figure 5.1. The 2-km ADAS winds barbs and wind speed contours at 10 m are displayed every hour on 19 February 1999 from 1400 UTC to 1900 UTC. Valid times are a) 1400 UTC, b) 1500 UTC, c) 1600 UTC, d) 1700 UTC, e) 1800 UTC, and f) 1900 UTC. A full barb indicates 5 m s^{-1} whereas a half barb is 2.5 m s^{-1}. Wind-speed thresholds are denoted by three levels of gray shading: 5.2 m s^{-1} (10 kts, lightest shade), 6.2 m s^{-1} (12 kts, intermediate shade), and 7.7 m s^{-1} (15 kts, darkest shade).
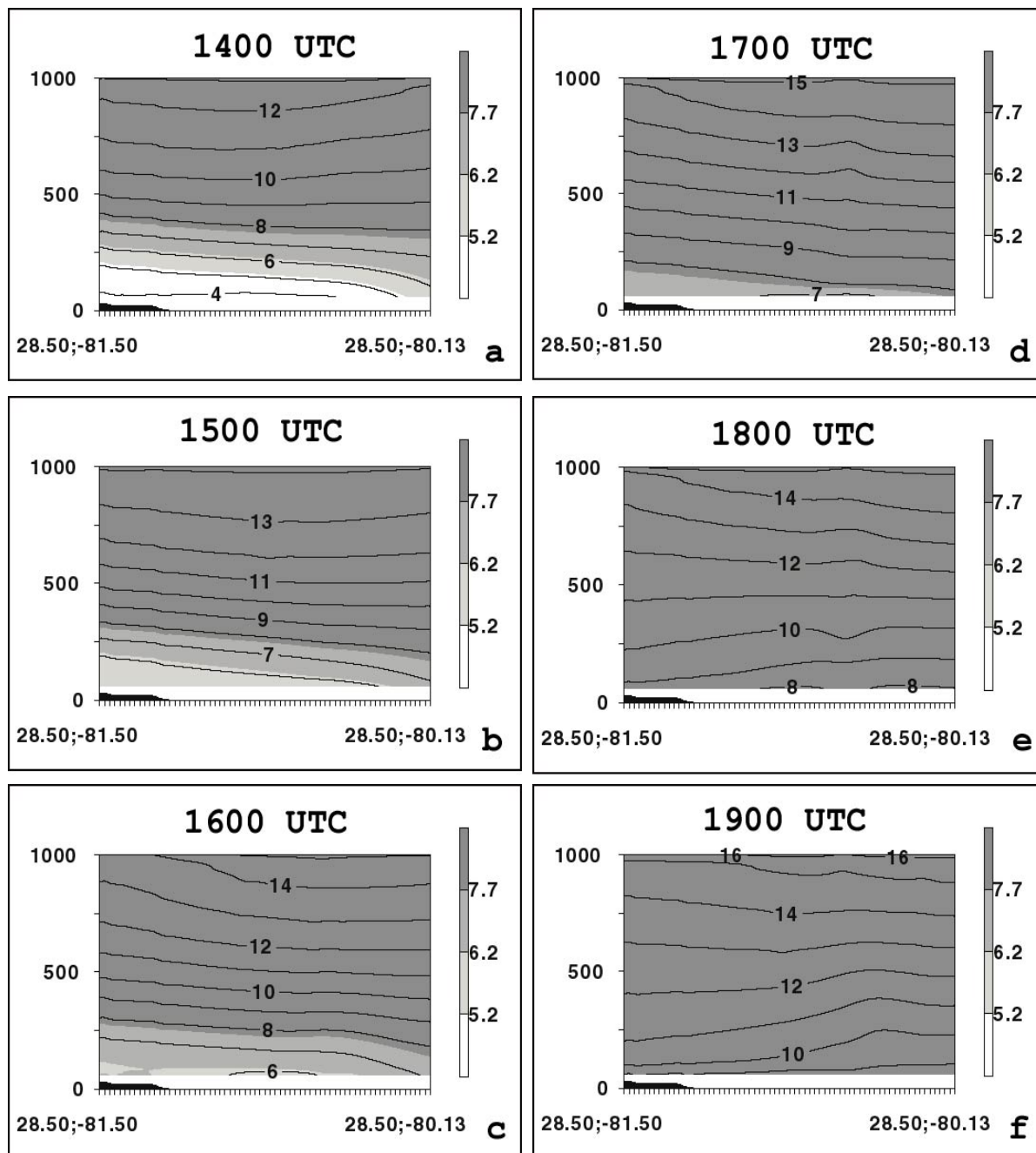
Figure 5.2. Cross sections of 2-km ADAS wind speeds are shown along the 28.5° latitude lines given in Figure 5.1. The vertical axis extends from the surface to 1000 m and wind speeds above 5.2 m s^{-1} (10 kts) are shaded according to the scale provided. Valid times for a)-f) are the same as in Figure 5.1.

The time evolution of the vertical wind profile at the SLF is depicted in Figure 5.3 for the time period from 1200 UTC to 2345 UTC 19 February. Between 1200 UTC and 1500 UTC, a strong vertical gradient in wind speed prevails from the surface to 700 m as speeds increase from 5−11 m s^{-1} in this layer. The lighter winds near the surface are generally from a south-southwest direction whereas the stronger winds aloft are from the west-southwest. Between 1500 and 1700 UTC, a wind shift occurs at low levels accompanied by an increase in wind speeds. By 1800 UTC, the vertical wind-speed gradient relaxes slightly as the winds become nearly unidirectional from the west-southwest in the entire layer. The vertical wind-speed gradient again increases in the lowest 500 m after 2000 UTC as wind speeds strengthen to > 15 m s^{-1} above 500 m.

20

In this particular case, the west-southwest winds at low levels were aligned perpendicular to the SLF runway which is oriented in a north-northwest to south-southeast direction. Thus, the magnitude of the total wind is a good approximation for the crosswind component at the SLF. However, in instances when the wind direction is aligned at a different angle to the SLF runway, the crosswind component (and correspondingly the head or tail wind components) can be easily computed by generating a cross section coincident with the SLF runway. The normal wind component in this hypothetical cross section represents the magnitude of the crosswinds at the SLF whereas the tangential wind component represents the magnitude of the head (tail) winds at the SLF. These products could be displayed as often as ADAS analyses are generated leading to a more complete and simplified assessment of the FR wind constraints.
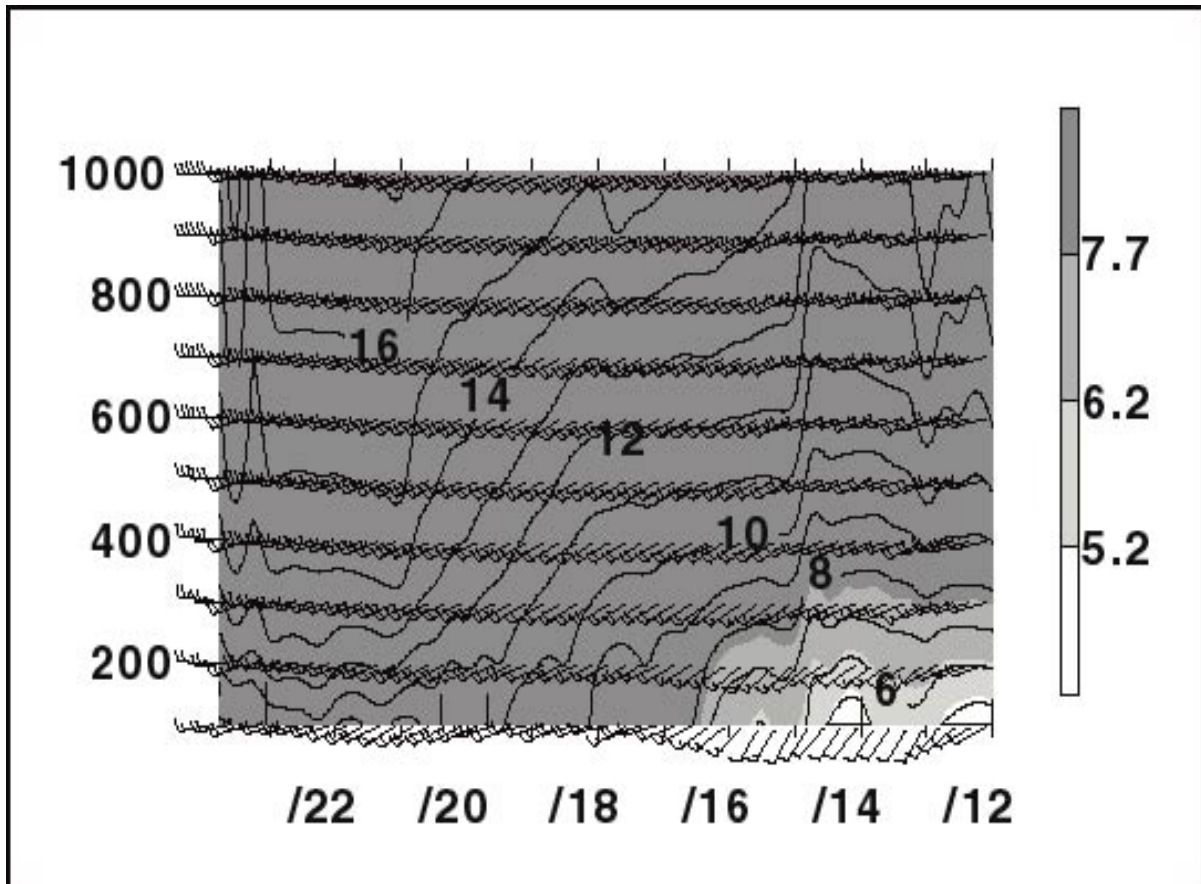
Figure 5.3.   A time-height cross section of 2-km ADAS wind speed and wind barbs is displayed at the NASA Shuttle Landing Facility from 1200 UTC to 2345 UTC 19 February. Time increases from right to left and wind speeds above 5.2 m s^{-1} (10 kts) are shaded according to the scales provided. The vertical coordinate is height in meters.

5.2 28 February 1999 (pre-frontal thunderstorms and cold frontal passage)

A strong southwest flow of warm, relatively moist air occurred ahead of a southeastward-moving surface cold front on this day. Temperatures reached the mid-upper 20s °C whereas dewpoint temperatures were in the mid 10s °C across east-central Florida ahead of a pre-frontal line of thunderstorms. The maximum convective available potential energy (CAPE, 1200–1600 J kg^{-1}) and minimum lifted indices (-5 to -6 °C) occurred along the west coast of Florida where surface dewpoint temperatures approached 20 °C. Over east-central Florida, the maximum CAPE was less than 1200 J kg^{-1} throughout the event. Wind speeds were strong throughout the troposphere including 10 m s^{-1} at the surface, 15 m s^{-1} at 850 mb, 25 m s^{-1} at 500 mb, and over 50 m s^{-1} at 300 mb. Winds veered with height from south-southwesterly at the surface to westerly at 500 mb and 300 mb. The combination of high vertical wind shear and moderate instability resulted in the development of a few strong to severe thunderstorms on this day.

WSR-88D base reflectivity data depicting the prefrontal line of thunderstorms is shown every half hour from 1813 UTC to 2044 UTC 28 February (Fig. 5.4). A southwest-northeast line of thunderstorms moved southeastward between 1813 UTC and 1913 UTC (Figs. 5.4a-c) approaching the northern portions of Merritt Island and KSC/CCAS by 1913 UTC. A particularly intense cell embedded in this line (labeled as #1), with reflectivities approaching 55 dBZ, pushed offshore to the north of KSC/CCAS. The squall line broke apart between 1913 UTC and 1943 UTC (Figs. 5.4c and d). At about 1943 UTC, two distinct cells developed to the southwest of KSC/CCAS (labeled as #2 and #3) and moved eastward into Melbourne at 2014 UTC (Fig. 5.4d-e). The broken line of convection continued to propagate southeastward and moved offshore to the east of KSC/CCAS and MLB by 2044 UTC (Fig. 5.4f).

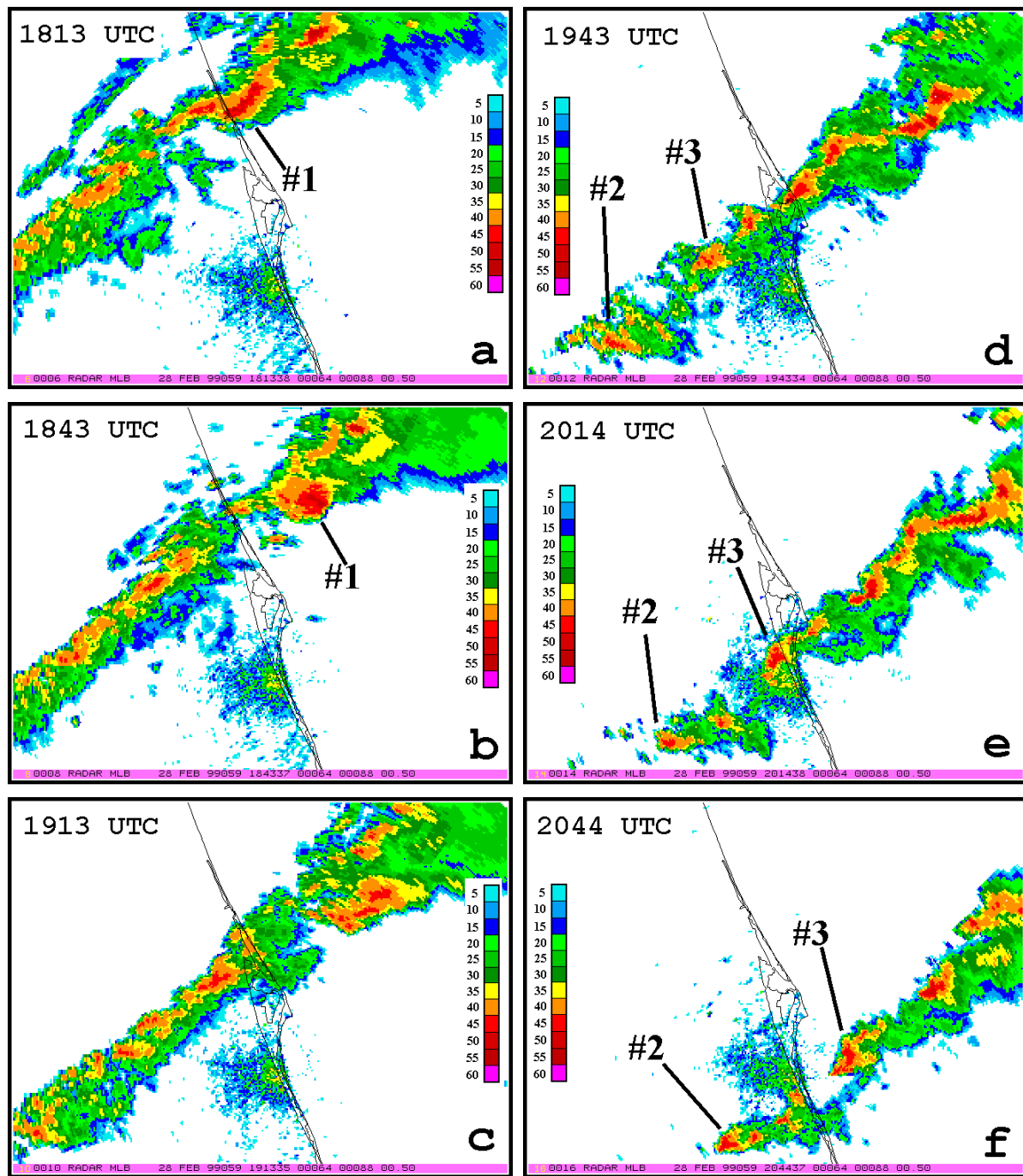Figure 5.4.   Base reflectivity images from the Melbourne WSR-88D are shown over east-central Florida from 28 February at the following times: a) 1813 UTC, b) 1843 UTC, c) 1913 UTC, d) 1943 UTC, e) 2014 UTC, and f) 2044 UTC.

23

One of the most valuable tools of ADAS for short-range quantitative forecasting of cloud properties is the CCS (complex cloud scheme) which is described in detail in the Appendix and Zhang et al. 1998. The cloud products empirically derived in ADAS provide a much easier means for assessing the quantitative properties of clouds such as ceilings, cloud-top heights, and cloud thicknesses, as compared to examining only GOES-8 imagery and WSR-88D data.

The 2-km ADAS-derived cloud-top heights and ceiling heights are given in Figures 5.5 and 5.6 respectively, and approximately correspond to the times in the base reflectivity images of Figure 5.4. It is important to note that the scales are different between the reflectivity images of Figure 5.4 and the cloud analyses of Figures 5.5 and 5.6. The cloud analyses are shown over the 2-km domain whereas the radar images of Figure 5.4 cover an area larger than the 2-km domain.

The anvils associated with the individual thunderstorms are clearly depicted in the sequence of cloud-top heights (Fig. 5.5). In particular, note the high cloud tops exceeding 12.5 km to the north and northeast of KSC/CCAS associated with cell #1 (labeled in Figures 5.4a and b and Figures 5.5a and b). The horizontal extent of the anvil associated with the squall line is illustrated by the nearly continuous band of high cloud-top heights in Figures 5.5a-c (> 7.5 km). As the squall line begins to break apart (Fig. 5.4d), the corresponding cloud-top height field also separates primarily to the southwest of KSC/CCAS (Fig. 5.5d). Finally, the anvils of two distinct areas of convection are depicted by cloud-top heights exceeding 7.5 km at 2015 UTC and 2045 UTC (Figs. 5.5e and f). These regions are labeled as cells #2 and #3 in Figures 5.4d-f and Figures 5.5d-f, respectively.

The ADAS-derived ceiling heights are shown in Figure 5.6 for the same times as in Figure 5.5. High cloud ceilings are analyzed at 1815 UTC, especially along the leading edge of the squall line where ceiling heights exceed 5 km in the vicinity of the thunderstorm anvil (Fig. 5.6a). Ceiling heights decrease to 250−500 m by 1845 UTC to the northwest of KSC/CCAS, whereas higher ceiling heights are diagnosed over the ocean northeast of KSC/CCAS (Fig. 5.6b). In Figures 5.6c-d, the highest ceilings continue along the leading edge of the line of storms while lower ceiling associated with the precipitation occur towards the back edge of the line of thunderstorms. Very low ceilings, less than 50 m in some locations, are analyzed in the vicinity of MLB at 2015 UTC associated with a severe thunderstorm (Fig. 5.6e). The areal coverage of analyzed ceilings decreases as the storms continue moving southeastward by 2045 UTC (Fig. 5.6f).

It is important to note that the quality and representativeness of the analyzed cloud fields are highly dependent on the available data that are integrated into ADAS. The analysis is only as representative as the quality and quantity of data that are ingested. Analysis fields can be misleading if the forecaster interpreting these fields does not have an understanding of the characteristics of the data being integrated. The transition of ceiling heights in Figures 5.6d-e provides a good example of how observational data influence the cloud analysis. The severe thunderstorm that moved through MLB originated over eastern Osceola county at 1945 UTC (Figure 5.6d) where no surface METAR observations of clouds are available. When the cell moved into the vicinity of the MLB METAR station, the combination of a special MLB observation and all other available data generated the very low ceiling analysis at 2015 UTC (Fig. 5.6e). This sequence of clouds analyses does not necessarily suggest that the ceiling suddenly decreased between 1945 UTC and 2015 UTC. In this instance, no METAR cloud observations were available at 1945 UTC to provide a report of low ceilings, resulting in the sharp transition in Figures 5.6d-e. This sharp transition illustrates the fact that the CCS of ADAS is limited to the quality, quantity, and location of the data that are ingested.
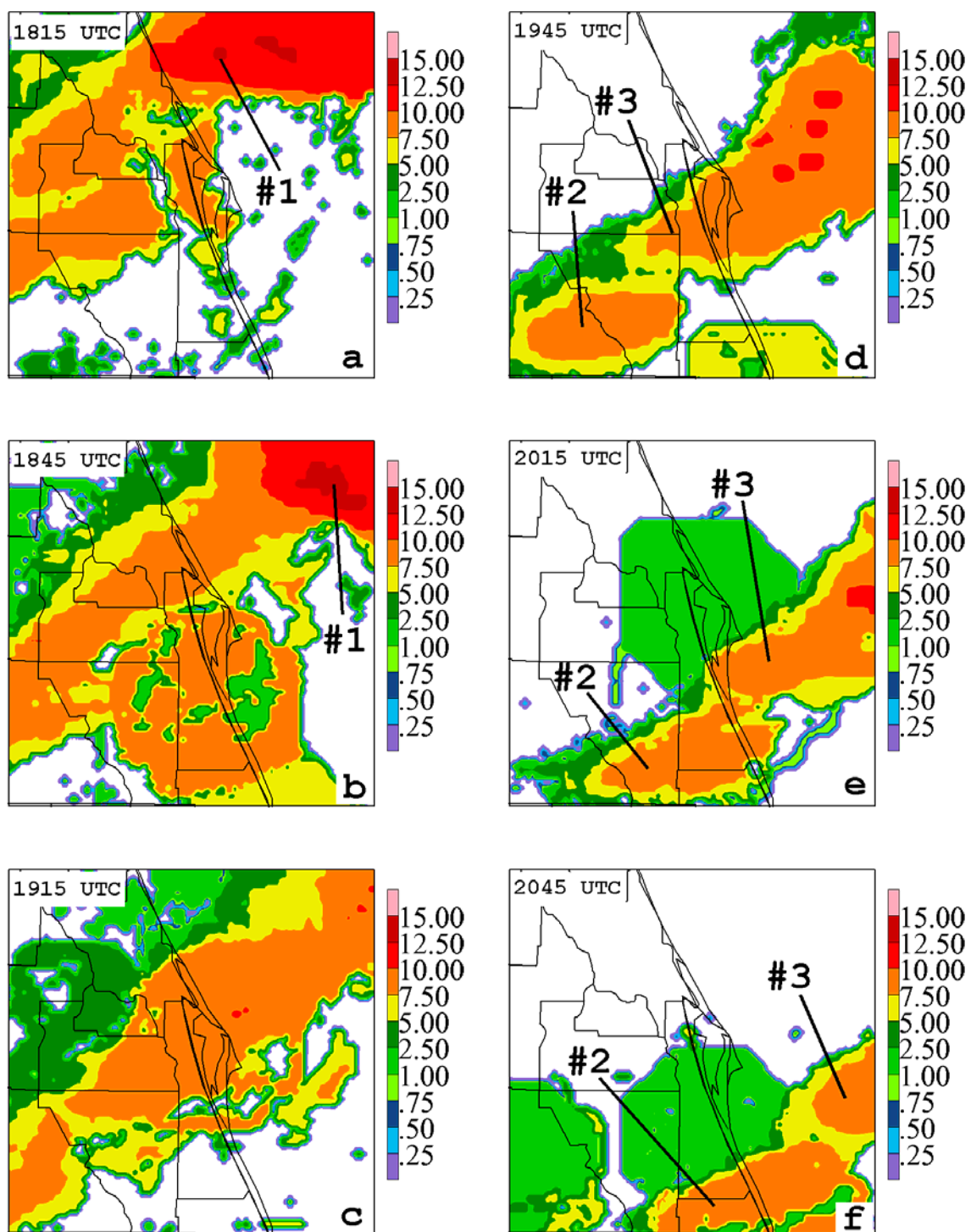
Figure 5.5. ADAS 2-km cloud top heights (km) are depicted according to the scale on the right hand side of each panel. Valid times are for 28 February at: a) 1815 UTC, b) 1845 UTC, c) 1915 UTC, d) 1945 UTC, e) 2015 UTC, and f) 2045 UTC.
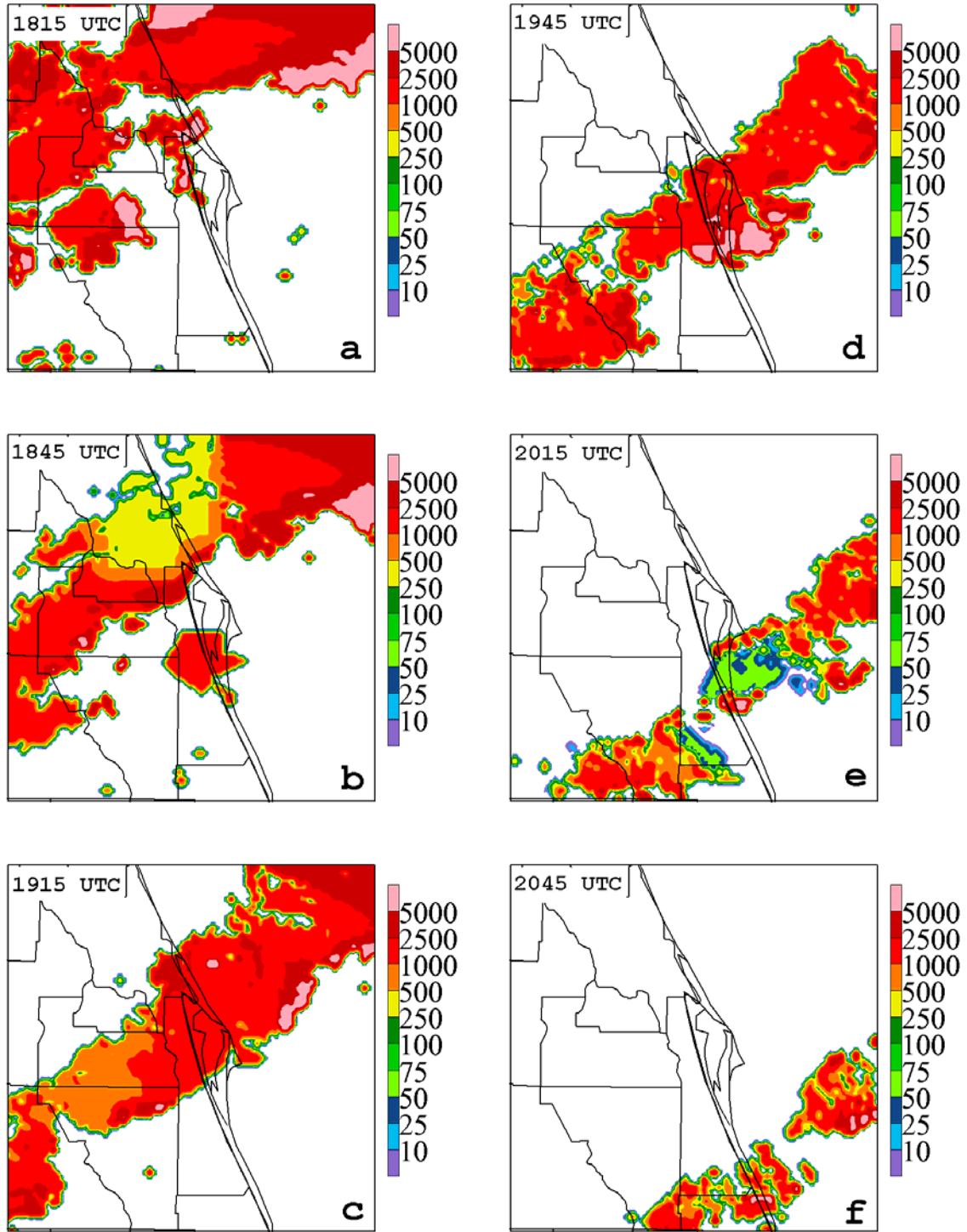
Figure 5.6.   ADAS 2-km ceiling heights (m) are depicted according to the scale on the right hand side of each panel. Valid times are for 28 February at: a) 1815 UTC, b) 1845 UTC, c) 1915 UTC, d) 1945 UTC, e) 2015 UTC, and f) 2045 UTC.

5.3 Summary of case studies

This section illustrated some of the capabilities of ADAS in a simulated real-time configuration through the presentation of two case studies from the two-week data archive. Other cases not shown from the two-week archive include a sea-breeze passage at the SLF on 17 February, low clouds and rain showers from 23 February, and other occurrences of FR and LCC violations related to wind and ceiling constraints. Based on a qualitative examination of graphics for each day, ADAS was able to routinely provide valuable analyses that could be used to diagnose a variety of weather events in support of space and ground operations at KSC/CCAS.

To summarize, while simulating a real-time configuration using data archived from 15−28 February 1999, ADAS demonstrated utility in the following weather situations.

- Depicting high-resolution quantitative characteristics of cloud fields such as ceilings, cloud-top heights, and cloud liquid, ice, and hail mixing ratios.

- Monitoring the magnitude of cross, head, and/or tailwind components at the SLF.

- Diagnosing a sea-breeze passage at the SLF (not shown). Low-level analyses every 15-minutes depicted the northwestward propagation of a sea-breeze boundary across KSC/CCAS.

- Assessing stability indices (CAPE, Lifted Index, Microburst Day Potential Index, etc.) at high temporal and spatial resolutions to determine thunderstorm risks (not shown).

6.0   System Sensitivities/Deficiencies

During the 2-week real-time simulation, ADAS ran reliably and the analyses were generally robust and accurate when all available data were ingested. The only times when analyses could not be generated resulted from missing RUC background fields. Additional shortfalls of the system occurred when certain observational data sets were missing or degraded, particularly those data that influence the complex cloud scheme. As part of the standard output, the amount and type of observations ingested into ADAS can be used to alert the forecaster as to the availability of data. As mentioned in the previous section, ADAS analyses are only as good as the amount and quality of the data that are ingested into the system.

This section discusses some of the problems and deficiencies that were encountered during the real-time simulation of LDIS. In particular, comparisons are made between the influence of level II versus level III WSR-88D data on the subsequent analyses. The deficiencies of the system as a result of using level III WSR-88D data are examined and the improved analysis fields are shown when utilizing the full-volume level II data. Also, examples are provided for instances in which no GOES-8 VIS and IR data were available at analysis times. An additional problem occurs with the derived cloud analysis fields shortly preceding sunset on 23 February due to the decreasing albedo in the VIS imagery as the sun angle lowered. Finally, within the two-week data archive, several RUC forecasts were missing for various three-hourly time intervals. Without the RUC as a background field, ADAS analyses cannot be generated for those specific time intervals. A simple solution is proposed which handles the missing RUC data problem.

6.1 Level II vs. Level III WSR-88D Data

6.1.1   Comparison of number of radial velocity observations

This section illustrates the impact that level III WSR-88D data have on the subsequent ADAS analyses as compared to level II WSR-88D data using all 14 elevation angles. The 28 February case is used for comparison because this day contained the greatest number of radar returns and therefore provides a good basis for the comparison study. The ADAS control simulation used level III WSR-88D data from all Florida radar sites. The analysis programs were then rerun for a nine-hour period (1500–2345 UTC) using level II data from only the MLB WSR-88D. Because the 2-km analysis grid contains radar data primarily from the MLB WSR-88D, all comparisons are made on the 2-km grid only, thereby isolating as much as possible the differences purely due to level II versus level III WSR-88D data.

In Section 3.1, a brief discussion was provided on the algorithm that remaps WSR-88D data onto the ADAS analysis grids. Insufficient volume coverage and large variance result in rejection of data at a particular grid location. Three factors lead to fewer remapped reflectivity and radial velocity observations using level III data compared to level II data.

- Because level II data contain all 14 elevation angles of data at a finer horizontal resolution compared to level III data, the areal coverage at a particular location on the ADAS grid is more substantial using level II data.

- More level II data are available at upper levels due to the higher elevation angles.

- Level III data experience larger variances because of the categorization of reflectivity and radial velocity into discrete bins.

Figure 6.1 illustrates the number of remapped radial velocity data points on the 2-km ADAS grid for both level II and level III WSR-88D data at each analysis time within the nine-hour comparison window. In general, the number of radial velocity observations on the 2-km ADAS grid using level II data greatly exceeds the number of radial velocity observations using level III data. The maximum number of remapped radial velocity observations is 7968 for level III data at 1930 UTC and 19631 for level II data at 1945 UTC (Fig. 6.1). A secondary maximum of remapped level III radial velocity observations occurs at 1800 UTC but is not prevalent in the level II data. This peak at 1800 UTC results from TBW and JAX level III data that are remapped onto the 2-km analysis grid in addition to the Melbourne level III data. However, only the MLB radar site was used to determine the number of remapped level II radial velocity observations.
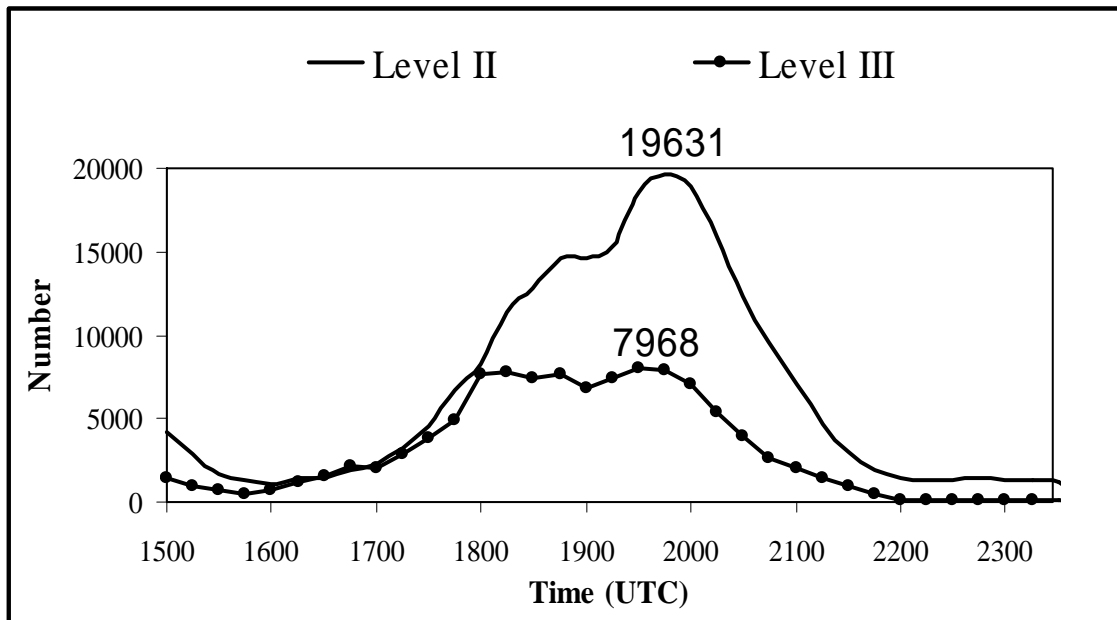
Figure 6.1. A plot of the number of radial velocity points remapped onto the 2-km ADAS analysis grid is given every 15 minutes on 28 February 1999 using all six Florida level III WSR-88D sites (labeled line) and level II data for the MLB WSR-88D site only (plain line).

6.1.2   Comparison of low-level frontal diagnosis

A consequence of the increased number of remapped radial velocity observations associated with level II data is the ability to detect more subtle boundaries and wind shift lines. This statement is supported by a diagnosis of the low-level cold frontal passage and its associated wind shift line using ADAS analyses ingesting level II versus level III WSR-88D data. The pre-frontal line of thunderstorms examined in Section 5.2 propagated through KSC/CCAS between 1900 UTC and 2000 UTC 28 February. The low-level cold front moved through KSC/CCAS at about 2200 UTC accompanied by a wind shift from southwest to west and no significant weather features (not shown).

Divergence plots at 870 m using level III data illustrate to a limited extent the areas of low-level convergence/divergence associated with the individual thunderstorms. At 2015 UTC, when a severe thunderstorm propagated through central Brevard county, a region of low-level convergence is depicted in the vicinity of the severe convection (Fig. 6.2a, corresponding to the reflectivity in Fig. 5.4e). Between 2030 UTC and 2100 UTC, small couplets of convergence and divergence are associated with the southeastward-moving line of convection (Figs. 6.2b, 6.3a-b). No other features in these plots suggest the approach of a low-level cold front and wind-shift line.

Many more small-scale details are present in the ADAS analyses using level II WSR-88D data. The convergence associated with the severe cell and nearby convection at 2015 UTC shows much more structure when using level II WSR-88D data (Fig. 6.2c). Beginning at 2030 UTC, a linear band of convergence develops to the northwest of KSC/CCAS with the approach of the cold frontal zone (Fig. 6.2d). This banded feature propagates slowly southeastward over the next 30 minutes reaching northern KSC/CCAS by 2100 UTC (Figs. 6.3c-d). The benefits of using level II WSR-88D data are quite obvious. Ingesting level II instead of level III data offers much more detail with regards to the wind features and areas of convergence associated with convection and the cold-frontal wind shift. The benefits of using level II data can be even more important during the Florida warm season when interactions between multiple outflow boundaries frequently occur.

Figure 6.2. Plots of ADAS 2-km divergence ($\times 10^{-5}$ s^{-1}) at 870 m are compared using level III WSR-88D data in a) and b), and level II WSR-88D data in c) and d). Shading represents convergence according to the scale provided whereas solid contours denote divergence. Valid times on 28 February are 2015 UTC in a) and c), and 2030 UTC in b) and d).
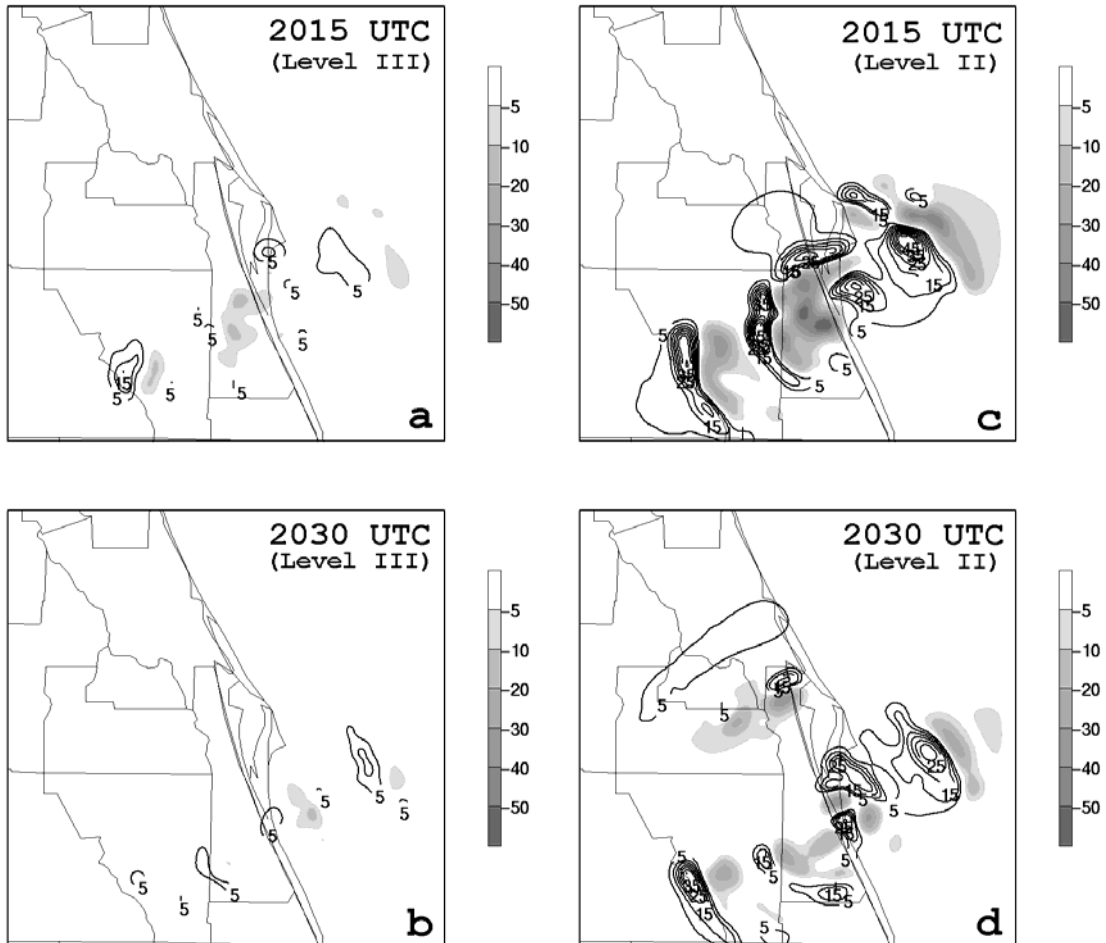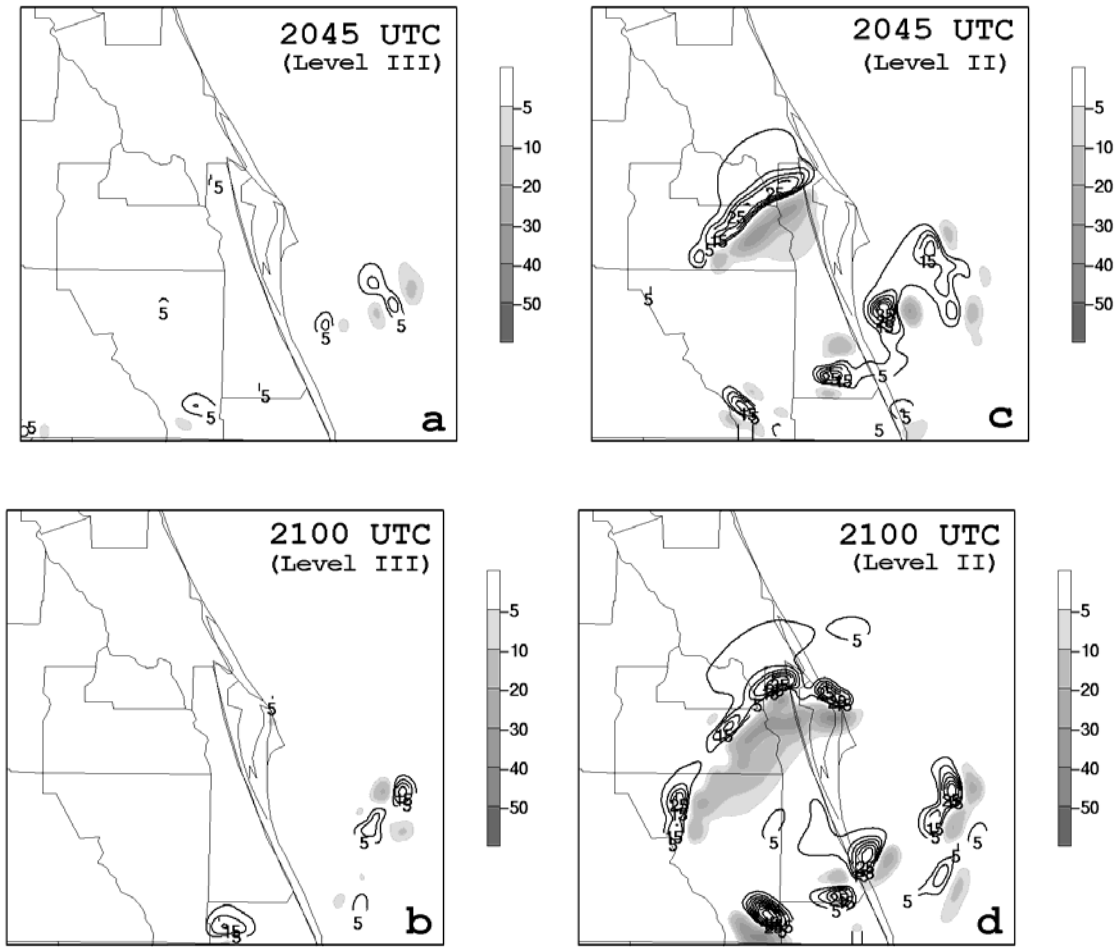
Figure 6.3. Plots of ADAS 2-km divergence ($\times 10^{-5}$ s^{-1}) at 870 m are compared using level III WSR-88D data in a) and b), and level II WSR-88D data in c) and d). Shading represents convergence according to the scale provided whereas solid contours denote divergence. Valid times on 28 February are 2045 UTC in a) and c), and 2100 UTC in b) and d).

6.1.3   Comparison of Cloud and Vertical Velocity Fields

Despite the greater volume of level II versus level III WSR-88D data, the impact of level II data on the cloud and moisture fields is rather insignificant on 28 February. This fact is illustrated through time-height cross sections of cloud liquid, cloud ice, and relative humidity fields at the SLF using level II versus level III data. The cloudiness associated with the passage of the pre-frontal line of convection is depicted in Figure 6.4a-b using level III and level II WSR-88D data respectively. With level III data, the ADAS-derived cloud liquid field extends from the surface to 350 mb whereas cloud ice extends from 550 mb to above 250 mb between 1900 UTC and 2000 UTC 28 February (Fig. 6.4a). Qualitatively, the derived cloud fields using level II data are very similar to the fields using level III data except that the cloud concentrations are slightly greater and the cloud liquid field extends to a higher level (~275 mb, Fig. 6.4b). The relative humidity fields using level III versus level II data (shaded regions in Figs. 6.4c and d respectively) are also nearly identical.

Since level II data have a greater influence on the horizontal winds than level III data, the impact on the vertical velocity field is also more significant. In ADAS, vertical velocities are derived by integrating the continuity equation using the horizontal winds at all vertical levels and top and bottom boundary conditions (w=0 at boundaries). The horizontal wind field is then adjusted / relaxed in order to conserve total mass

divergence (Brewster 1996). The differences in the ADAS-derived vertical velocity fields using level III versus level II data are shown in Figures 6.4c and d. At 1930 UTC, a deep area of rising motion associated with the squall line passage (maximum > 30 cm s^{-1}) is analyzed between 850 mb and 250 mb using level III data (Fig. 6.4c). However, the same time-height cross section using level II data reveals a much more intense updraft between 850 mb and 350 mb (maximum > 75 cm s^{-1}) as well as a downdraft on the trailing edge of the squall line (Fig. 6.4d). Sinking motion exceeds -100 cm s^{-1} in the mid-upper troposphere at 1945 UTC and extends down to near the surface at a lesser magnitude by 2000 UTC (dashed contours in Fig. 6.4d). Operationally, it is important to be able to diagnose regions of strong subsidence associated with convective activity because this sinking motion can lead to strong low-level horizontal winds as observed in this particular case.

Despite the degradation in horizontal resolution and fewer observed elevation angles, a significant benefit gained by ingesting level III WSR-88D data from all Florida radar sites is the increased horizontal coverage of radar data. As opposed to using level II data from only the MLB site, areal coverage of level III data includes most of the Florida peninsula and panhandle (Fig. 2.2a). This increase in coverage is most valuable on the 10–km analysis grid. Data from multiple radar sites on 28 February contributed favorably to the time-continuity of analyzed cloud and vertical velocity fields on the 10-km grid (not shown). The different aspects of level II versus level III WSR-88D data further supports the fact that an LDIS user should be aware of the characteristics of data ingested into the analysis system in order to utilize the results appropriately.
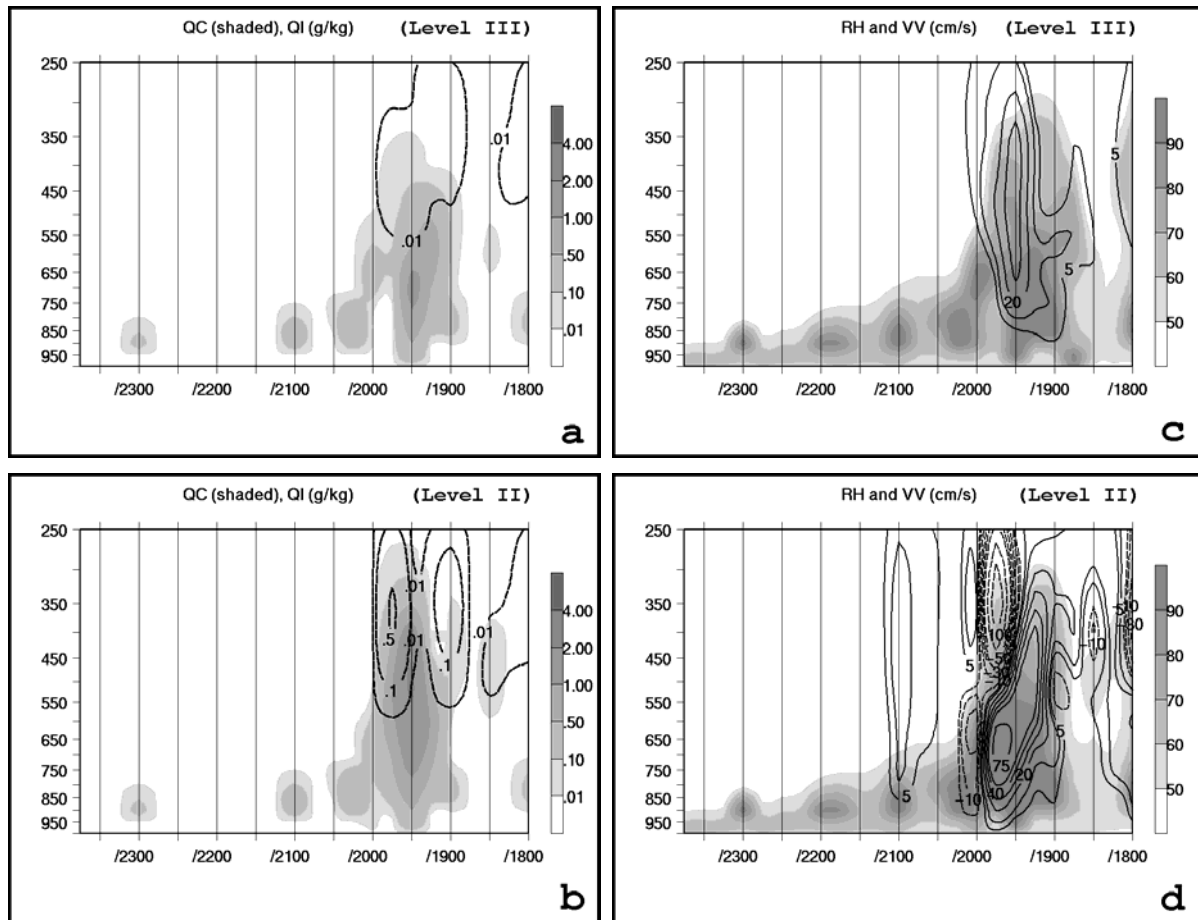
Figure 6.4.   Time-height cross sections illustrating the influence of level II versus level III WSR-88D data are displayed from 1800 UTC to 2345 UTC 28 February. ADAS-derived cloud liquid (QC, × 10^{-3} g kg^{-1}, shaded according to the scale provided) and cloud ice (QI, contoured, × 10^{-3} g kg^{-1}) fields are shown using a) level III WSR-88D data and b) level II WSR-88D data. ADAS-derived relative humidity (RH, shaded in % according

to the scale provided) and vertical velocity (cm s^{-1}, dashed contours indicate negative values or sinking motion) fields are shown using c) level III WSR-88D data and d) level II WSR-88D data.

6.2 Missing / Deficient GOES-8 Data

Based on the real-time data stream at SMG, GOES-8 imagery are not received during synoptic times (e.g. 0000 UTC, 0300 UTC, 0600 UTC, etc.). As a result, the cloud fields derived from the CCS of ADAS are deficient during these and other times of missing satellite data especially when no significant WSR-88D reflectivity data are available. In this situation, the primary data source that contributes towards the cloud analyses is METAR cloud reports.

Two examples of analyzed cloud ceilings without the influence of GOES-8 IR and VIS data are shown in Figure 6.5 from 1800 UTC and 1830 UTC 23 February. At 1800 UTC, several different METAR stations reporting ceilings (broken or overcast) contribute to the analyzed pattern in Figure 6.5a. The blocky nature of the analyzed cloud fields is caused by the influence radius being applied to each individual cloud observation including the stations that report clear or scattered clouds. A single special observation reporting a ceiling is depicted in the 1830 UTC analysis (Fig. 6.5b). These results show that the cloud analysis depends heavily upon the presence of GOES-8 satellite data for an accurate and high-resolution depiction of the cloud fields.

In the final step of the ADAS CCS, GOES-8 1-km VIS data are used to remove excess areas of cloud cover based on a comparison between the VIS imagery and the existing ADAS cloud cover field (see Appendix). A cloud albedo field is derived from VIS imagery and the albedo field is then compared to the ADAS gridded cloud cover. Excess cloud cover is removed from the ADAS cloud fields in order to match the albedo fields. Since VIS data are not available at night, the analyzed cloud cover can be too widespread.

This final step in the CCS can also lead to problems when the sun angle is low near sunrise and sunset. During these times, albedo data become unreliable and can negatively influence the cloud analysis by removing too much cloud cover. This problem is corrected within the CCS by withholding VIS data when the sun angle is lower than a specified threshold. As a result, sharp transitions in the analyzed cloud field can occur from one analysis time to the next once VIS data are no longer used in the CCS.

Such a sharp transition occurs on 23 February between 2115 UTC and 2215 UTC as the sun angle traverses below the specified threshold angle. The sequence of GOES-8 VIS images are given in Figure 6.6 and the corresponding ADAS-derived ceilings are shown in Figure 6.7. A widespread area of cloud cover lies across east-central Florida at 2115 UTC (Fig. 6.6a) and drifts slowly southward over the next hour (Fig. 6.6b-d). Patchy cloudiness is found over the northeastern portion of the Florida peninsula. It is important to note the decrease in albedo as indicated by the darkening of the VIS imagery with time.

Figure 6.5. ADAS-derived ceiling heights (m) on the 2-km analysis grid are indicated according to the scale on the right hand side of each panel. Valid times are for 23 February at: a) 1800 UTC and b) 1830 UTC.

The 10-km ADAS analyses do not depict any ceilings at 2115 UTC and 2130 UTC (Fig. 6.7a-b) despite the cloud cover indicated by the VIS imagery in Figures 6.6a-b. It is possible that the derived albedo information is already deficient and causes all analyzed ceilings to be removed as a result. By 2200 UTC, cloud ceilings are analyzed across only the oceanic regions to the east of Florida (Fig. 6.7c). Note that the sharp western edge of the derived ceilings is bounded by a north-northwest to south-southeast line. This boundary represents the sun angle threshold that is applied to the VIS cloud clearing algorithm. To the east of this line the sun angle is lower than the threshold and, thus, cloud cover is not removed by the VIS data. Conversely, to the west of this line the sun angle is above the threshold and, thus, cloud cover is removed based on the VIS-derived albedo data. Finally, cloud ceilings are analyzed over all portions of the 10-km analysis domain at 2215 UTC as VIS data are no longer used in the analysis (Fig. 6.7d).
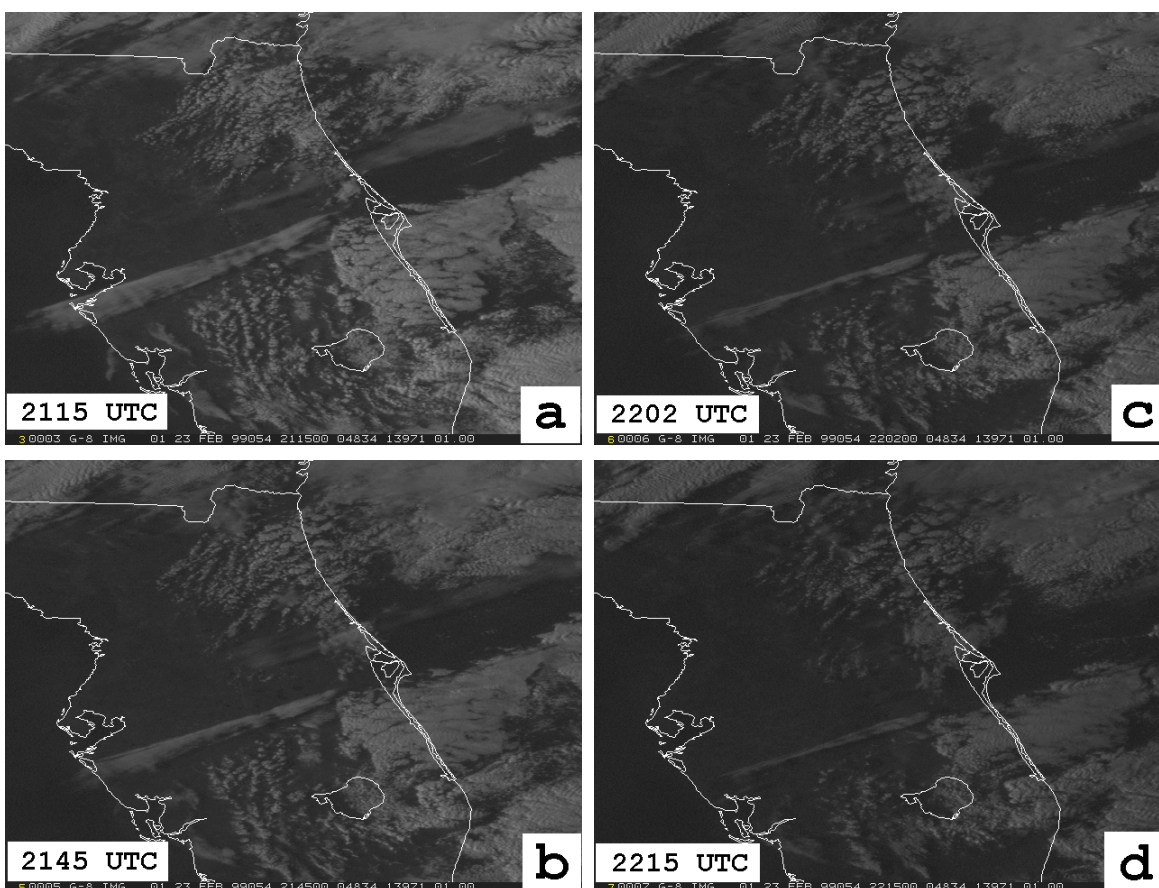
Figure 6.6.   The 1-km resolution GOES-8 visible imagery is shown for times of low sun angle prior to sunset on 23 February. The valid times are a) 2115 UTC, b) 2145 UTC, c) 2202 UTC, and d) 2215 UTC.
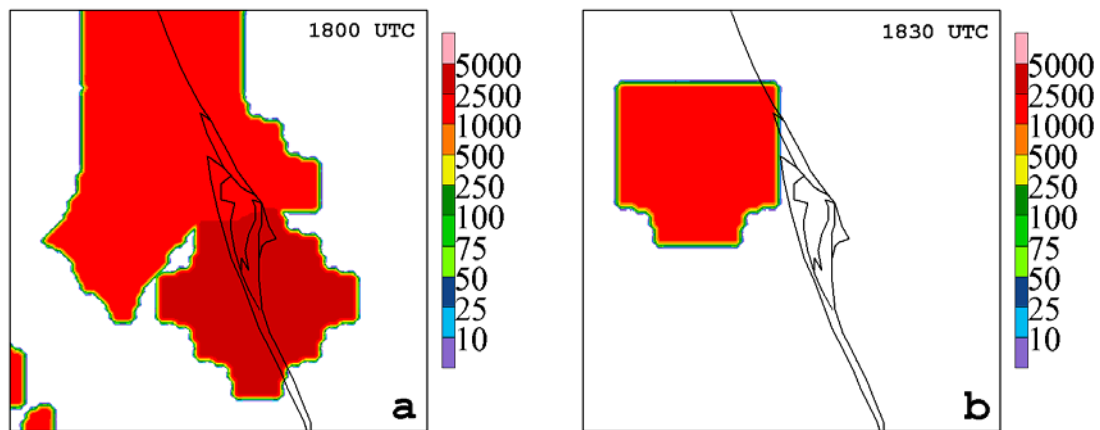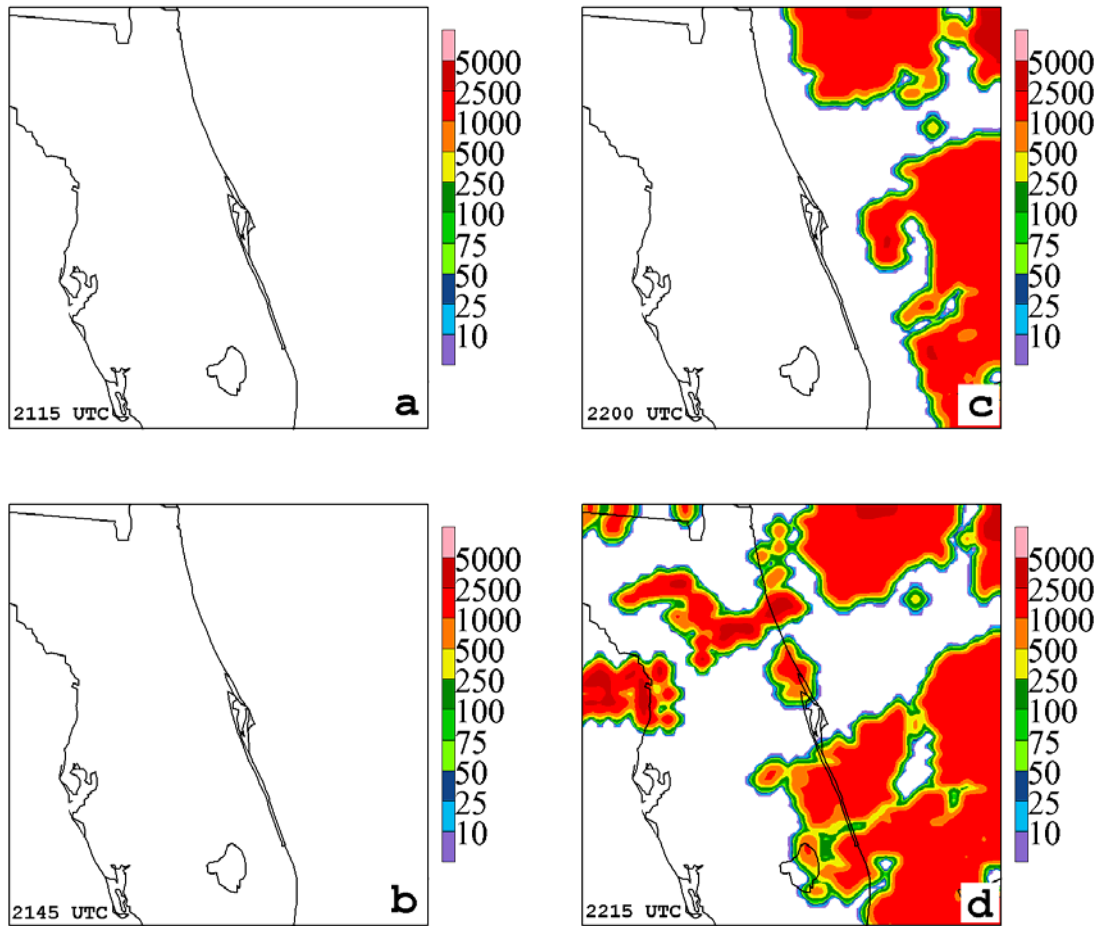
Figure 6.7. ADAS-derived ceiling heights (m) on the 2-km analysis grid are indicated according to the scale on the right hand side of each panel. Each ceiling plot of this figure corresponds to the respective visible imagery in Figure 6.6. Valid times are for 23 February at: a) 2115 UTC, b) 2145 UTC, c) 2200 UTC, and d) 2215 UTC.

6.3 Missing RUC forecasts

As discussed in Sections 2.2.2 and 2.3.1, an ADAS pre-processing program is used to interpolate RUC forecast gridded data onto the 10-km ADAS analysis grid. The RUC 3−6-h forecasts serve as background fields for the subsequent 10-km ADAS analyses. While converting the RUC data from the real-time archive onto the 10-km ADAS grid, specific times occurred when RUC forecast data were missing. For the real-time LDIS simulations, only RUC 0−6-h forecast grids were archived. Therefore, no ADAS analyses could be generated for certain three-hour intervals when the 3-h and/or 6-h RUC forecast data were missing.

This problem can be corrected by using an older RUC or Eta forecast grid as a background field for ADAS. If the 3−6-h forecasts are missing from a certain RUC model run, then the 6−9-h forecasts from the previous 3-hourly RUC cycle can be used as background fields for the subsequent 10-km ADAS analyses. This process can be extended back one more 3-h cycle to RUC 9−12-h forecasts. If three consecutive RUC forecast cycles are missing the procedure will have to resort to another model simulation such as the Eta 0−12-h or 12−24-h forecasts interpolated temporally to the ADAS analysis times of interest. To generalize, if any model is available that contains forecast grids valid at the analysis times of interest, it is possible to interpolate these model forecast grids to the 10-km ADAS grid.

7.0   Data Non-Incorporation Experiments

In a similar manner to LDIS Phase I, data non-incorporation (DNI) experiments are conducted for specific data sets to measure quantitatively the impact of various observations. In LDIS Phase I, DNI tests were performed on two specific case studies by withholding groups of data sets that measured similar meteorological quantities and possessed similar spatial and temporal characteristics. New analyses were generated and compared to the control analyses which included all data sources.

In the current study, DNI tests are run for only three specific data sets that experience a significant latency between the time of observation and time of receipt at SMG (Table 7.1). These data sets include rawinsonde data for all Florida sounding sites except the Cape Canaveral rawinsonde (RAO), GOES-8 satellite soundings (SAT), and GOES-8 water vapor and cloud drift winds (SWN). In order to simulate a possible real-time configuration, these three data were withheld from the control simulation of the two-week period of 15-28 February 1999 (see Section 2.3.3). Therefore, unlike the LDIS Phase I DNI experiments, analyses were re-run by individually including these three data sets described above. However, the methodology applied to the current DNI experiments yields the same type of information about the relative impact of the data as in LDIS Phase I.

It is important to note that because a much larger sample size is used for LDIS Phase II, the DNI results given in this report represent a more rigorous test of the impact of each data set compared to the LDIS Phase I DNI experiments. Whereas the DNI tests were conducted for two 8-h periods in LDIS Phase I, the current DNI tests are run over a 336-h period (2 weeks) in the current experiment. Thus, the much larger data sample provides a more representative assessment of the average impact of each data source. However, these experiments demanded an extensive amount of computational resources and required about one week of wall-clock time to complete each DNI test. Thus, the experiments were conducted only for the data sources with real-time data latency problems.

As in the LDIS Phase I report, spatial correlation coefficients (CCs) are computed between the control analysis and each DNI run. Spatial CCs measure the degree to which patterns are similar between two fields (Anthes 1983). Values of CCs range from –1 to 1 where 1 indicates exact agreement while 0 indicates no correspondence. For CCs of –1, the scalar patterns have the same shape and gradients but opposite sign.

There are several factors that can result in a CC near unity.

- DNI observational data can be nearly identical to the background field.

- DNI observational data may be few in number or receive small weights.

- DNI observations can be rejected during the quality control algorithms.

- The DNI analysis may have nearly identical patterns and gradients to the control analysis, but experience a change in magnitude across much of the domain.

It is important to note that CCs alone are not sufficient to measure quantitatively the collective influence of a specific data source. In some instances, two analysis fields may be highly correlated with similar scalar patterns and gradients, yet experience a significant difference in magnitude over the entire domain. Such a magnitude change could result from an inherent instrument bias or a poor background field, for example. Additional statistical variables such as root mean square error are required to measure the magnitude changes between two fields in addition to differences in patterns and gradients. However, only CCs are examined in the current set of experiments.

The CCs are computed for the analyzed u- and v-wind components, moisture (RH*), potential temperature (θ), and pressure (p). The CCs are calculated at every ADAS vertical level for both the 10-km and 2-km analyses, but only over the 2-km horizontal domain. The DNI data sets tested do not typically influence every ADAS vertical level. Thus, the DNI experiments are designed to isolate the portions of the analysis that are influenced the most by the DNI data set. As a result, CCs for all ADAS vertical levels are sorted and the four smallest CCs are averaged for every 15-minute analysis cycle. These four-level CC-means are then averaged over the entire two-week period of the experiment only for analysis times that contain observations from the DNI data source. CC-means and standard deviations for the 2-km subset of the 10-km analysis and for the 2-km analysis are given in Tables 7.2 and 7.3, respectively.

Table 7.1.   A list of the data non-incorporation (DNI) experiments is shown consisting of the DNI name, the data source included for each test, and the analysis variables that are influenced directly by the respective data source.

DNI Name	Data Source Included	Analysis Variables Affected
RAO	All Florida rawinsondes except XMR	u, v, RH*, θ, p
SAT	GOES-8 derived satellite soundings	RH*, θ, p
SWN	Satellite-derived winds	u, v

Table 7.2.   The mean and standard deviation of correlation coefficients for each data non-incorporation (DNI) run is provided for a subset of the 10-km analysis grid covering the 2-km analysis domain. The notation used in each column is mean/standard deviation or N/A for items not applicable because the analysis variables are not measured by the data source. See text for further details.

Analysis Variable	RAO Mean	RAO St. Dev.	SAT Mean	SAT St. Dev.	SWN Mean	SWN St. Dev.
u	0.883	0.125	N/A	N/A	0.869	0.131
v	0.925	0.080	N/A	N/A	0.890	0.111
RH*	0.889	0.115	0.550	0.423	N/A	N/A
θ	0.891	0.116	0.667	0.326	N/A	N/A
p	0.971	0.032	0.928	0.077	N/A	N/A

Table 7.3.   The mean and standard deviation of correlation coefficients for each data non-incorporation run is provided for the 2-km analysis grid. The notation used in each column is mean/standard deviation or N/A for items not applicable because the analysis variables are not measured by the data source. See text for further details.

Analysis Variable	RAO Mean	RAO St. Dev.	SAT Mean	SAT St. Dev.	SWN Mean	SWN St. Dev.
U	0.925	0.093	N/A	N/A	0.922	0.086
V	0.946	0.078	N/A	N/A	0.936	0.078
RH*	0.919	0.093	0.610	0.372	N/A	N/A
θ	0.949	0.071	0.727	0.277	N/A	N/A
P	0.975	0.041	0.940	0.064	N/A	N/A

7.1 Florida Rawinsondes

The Florida rawinsonde data set (RAO) consists of all rawinsondes in Florida except the Cape Canaveral rawinsonde (XMR). The RAO experiences as much as a 2-h latency between observation and receipt time at SMG (Table 2.1), however, the XMR rawinsonde is received in near real-time. Thus, only the Florida rawinsondes outside of KSC/CCAS are benchmarked in the RAO DNI experiment.

Among the three data sources with a significant real-time latency, the RAO is the only data set that impacts all analyzed variables directly. On average, the influence of the RAO on each analyzed variable is relatively insignificant due to the small number of rawinsonde observations affecting the ADAS 10-km and 2-km domains. The smallest average CCs occur on the 10-km analysis grid and include the analyzed u-wind component, moisture (RH*), and potential temperature (θ). The mean CCs range from 0.883–0.891 on the 10-km analysis grid for these variables and 0.919–0.949 on the 2-km grid (Tables 7.2 and 7.3). The analyzed v-wind component and especially the pressure patterns are on average affected the least by the RAO with mean CCs as high as 0.946 for the v-wind component and 0.975 for pressure on the 2-km grid.

The average variability of CCs as determined from the standard deviation for each analyzed variable is also relatively small in all instances. The maximum standard deviation for any analyzed variable is 0.125 for the u-wind component on the 10-km grid. A small variability in CCs indicates that CCs are typically close to the mean value. The combination of highly correlated analysis fields and small variability of the CCs during the two-week DNI test suggests that RAO observations generally do not significantly alter the patterns of analyzed variables. Therefore, given the real-time latency of RAO and the DNI evidence suggesting that the RAO do not strongly impact the patterns of analyzed variables, it is perhaps prudent to withhold the RAO data in a real-time LDIS configuration.

7.2 GOES-8 Satellite Soundings

Vertical profiles of temperature and moisture are retrieved hourly from GOES-8 sounder data with a horizontal resolution of approximately 30 km (Gray et al. 1996). GOES-8 satellite soundings do not retrieve winds, therefore, only the analyzed temperature, moisture, and pressure fields are directly affected in the ADAS analyses. GOES-8 soundings are available only in cloud-free regions so horizontal coverage can vary depending on the amount of cloud cover and synoptic conditions. GOES-8 retrieved soundings of temperature and moisture are available once per hour at about 10-15 minutes past the hour. Due to the retrieval process and necessary algorithms, these data are not available in real-time and typically experience about a 50-minute lag between observation and receipt time at SMG (Table 2.1).

Unlike RAO observations, GOES-8 soundings (SAT) have a more pronounced impact on the analyzed moisture (RH*) and potential temperature (θ) fields. The smallest average CC for the SAT DNI experiment is 0.550 (0.610) for RH* on the 10-km (2-km) analysis. CCs for θ are also comparably smaller than in the RAO DNI experiment with a average value of 0.667 (0.727) on the 10-km (2-km) analysis (Tables 7.2 and 7.3). The SAT CCs for RH* and θ are noticeably smaller than the corresponding RAO CCs which are generally 0.25–0.35 higher. These smaller mean CCs suggest that incorporating SAT leads to a fairly substantial change in the analyzed patterns of temperature and moisture compared to the control and RAO ADAS analyses.

The average variability of SAT CCs is substantially larger than the average variability in RAO CCs as given by the standard deviations in Tables 7.2 and 7.3. The average standard deviations for RH* and θ are nearly three to four times larger for SAT than for RAO. This amount of variability in SAT CCs indicates that CCs near 0 or 0.1 can occur as frequently as CCs in the 0.8–1.0 range. Graphs of the individual CCs on the 10-km and 2-km analyses for the two-week period indicate that several instances of CCs below 0.2 occur including several negative values in the -0.2 to -0.4 range especially for RH* (not shown). The physical significance of a negative CC on the moisture or temperature analysis fields indicates a reversal in the direction of the scalar gradients. Since many instances of small or negative CCs occur in the SAT DNI experiment, this data set often changes the patterns of analyzed temperature and moisture substantially from the background field. Further investigation is necessary to determine the quality of these analysis modifications due to GOES-8 soundings, however, it is beyond the scope of the current study.

7.3 GOES-8 Cloud Drift / WV Winds

The third DNI experiment consists of a combination of GOES-8 cloud drift and water vapor (WV) winds. Only the analyzed u- and v-wind components are affected by these data sets. The vertical and horizontal distribution of cloud-drift winds depends on tracking cloud features and diagnosing heights to assign the vertical level for the associated wind (Neiman et al. 1997). The coverage of WV winds also depends on tracer selection and height assignment, although WV wind vector targets are selected in both cloudy and cloud-free regions (Veldon et al. 1997). In contrast to GOES-8 soundings, cloud-drift and WV winds are found where clouds and moisture features can be readily identified by the tracer selection and tracking algorithms (Neiman et al. 1997; Veldon et al. 1997). Cloud drift winds are assigned heights at high- (100–400 mb), middle- (400–700 mb) and low- (700–950 mb) levels (Neiman et al. 1997) while WV winds are assigned heights at levels between 250–600 mb (Veldon et al. 1997).

Based on the results from this DNI experiment, GOES-8 cloud drift and WV winds (SWN) have a marginal impact on the analyzed patterns of u- and v-wind components. The average CCs are all greater than 0.86 on both the 10-km and 2-km analyses (Tables 7.2 and 7.3). In addition, the standard deviation of CCs during the two-week period is relatively small indicating that for most analysis times affected by SWN, the impact on the patterns of analyzed wind components is small. Therefore, based on the relatively small impact of SWN on both the 10-km and 2-km analysis grids and the large real-time latency in Table 2.1, it is most likely prudent to withhold SWN observations from a real-time LDIS configuration.

7.4 Comparison between 10-km and 2-km DNI results

A feature of the DNI experiments that showed up in each run is that CCs are all smaller and most standard deviations are larger on the 10-km analysis (computed only over the 2-km domain) compared to the 2-km analysis (Tables 7.2 and 7.3). At first glance, these statistics may seem unusual since CCs are computed only on the area covering the 2-km domain for both grids. However, the 2-km subset of the 10-km analysis has fewer grid points than the 2-km analysis. Fewer grid points in conjunction with a larger influence range (Table 2.2) cause a larger percentage of grid points to be affected by the observational data on the 2-km subset of the 10-km analysis. Therefore, CCs are generally smaller on the 2-km subset of the 10-km analysis rather than the 2-km analysis.

8.0   Summary and Future Direction

A simulation of a real-time Local Data Integration System (LDIS) was conducted for a two-week data archive from 15-28 February 1999. The Advanced Regional Prediction System (ARPS) Data Analysis System (ADAS) was used for the real-time simulation on the same IBM RS/6000 hardware platform as used in the LDIS Phase I study. Many aspects of the original LDIS configuration from Phase I remained the same including the two nested grids with 10-km and 2-km resolutions respectively, the 15-minute analysis cycle frequency, and the ingest window that incorporates data at ± 7.5 minutes centered on each analysis time.

Several modifications to the LDIS configuration were necessary in order to simulate a real-time configuration.

- Rapid Update Cycle (RUC) forecasts rather than analyses were used as background fields for the 10-km ADAS analyses.

- Level III rather than level II WSR-88D data were ingested into ADAS since level III data are received in real-time at SMG.

- Level III WSR-88D data from all Florida sites were used rather than level II WSR-88D data from only the Melbourne radar site as in LDIS Phase I.

- Three data sources (satellite soundings, satellite-derived winds, and Florida rawinsondes other than the Cape Canaveral sounding) were not included in the control simulation of the real-time LDIS due to the large latency between the time of observations and the time of receipt at SMG.

- The multiple-pass configuration of ADAS was performed in four iterations of the Bratseth objective analysis scheme for both the 10-km and 2-km analyses.

8.1 Summary of Real-time Data Characteristics

In Section 3, the characteristics of the archived real-time data sets used in the control simulations were examined. In addition, Section 7 provided an analysis of the data sets that were not used in the control simulations by conducting data non-incorporation (DNI) experiments to measure the relative impact that these data sources have on the subsequent patterns of analyzed variables. Based on the results presented in these sections, the following summary is given on the real-time data archive.

- Among the available data in real-time, KSC/CCAS tower and profiler observations, and WSR-88D data consistently provide the most numerous mesoscale observations at each analysis time.

- Many more WSR-88D reflectivity and radial velocity data points are remapped onto the 2-km analysis grid rather than the 10-km analysis grid. This result is due to the smaller size of an individual 2-km grid volume compared to a 10-km grid volume. The smaller 2-km volume results in a greater percentage of coverage of WSR-88D data, a smaller variance within the grid volume, and thus a smaller amount of rejected data.

- Level III WSR-88D as received at SMG are characterized by:

  - 1-km horizontal resolution.

  - The four lowest elevation angles at Melbourne only; the lowest two elevation angles at all other Florida radar sites.

  - Sixteen categorized numerical values for both reflectivity and radial velocity data.

- Level II WSR-88D are characterized by:

  - Gate-to-gate horizontal resolution of 250 m along a given radial.

  - All fourteen elevation angles during volume coverage pattern 11.

  - No categorization of numerical values.

- DNI experiments revealed that among the data sources with large real-time latency, GOES-8 sounding data have the most substantial impact on the analyzed patterns of temperature and humidity. Due to the extensive amount of observations in cloud-free regions, GOES-8 soundings can provide the most utility to ADAS analyses compared to other data sources that experience large real-time latency.

- Satellite-derived winds only slightly influence the patterns of analyzed u- and v-wind components.

- Florida rawinsondes affect the patterns of all analysis variables but only to a small extent.

8.2 Summary of Hardware Recommendations

The AMU ran the two-week real-time LDIS simulation on an IBM RS/6000 workstation with a 67 MHz clock rate and 512 MB of memory. The average wall clock time for each 15-minutes analysis cycle was 7.29 minutes, not including data pre-processing and graphical post-processing. Therefore, the analysis configuration used on the IBM RS/6000 workstation runs in real-time but is not sufficiently fast for an operational mode unless all pre- and post-processing were simultaneously conducted on a separate workstation.

In order to obtain analysis products in an operationally useful time frame, SMG specifications require that the entire analysis cycle, including pre-and post-processing, is completed in about 5 minutes. The AMU estimates that the following hardware and software characteristics will be required to run the LDIS Phase II configuration in 5 minutes or less.

- A workstation with at least a 200-MHz processor to run LDIS three times faster than the workstation used by the AMU. A multiple processor machine would further decrease wall clock time through the optimization of executable code.

- A workstation with at least 512 MB of memory.

- A configuration in which pre-processing programs and graphical post-processing programs are run on a separate workstation. A workstation with less CPU speed would be necessary to run the LDIS cycle in SMG's specified time if the pre- and post-processing were performed on separate a workstation.

8.3 Summary of Real-time LDIS Utility

While simulating a real-time LDIS configuration using data archived from 15–28 February 1999, ADAS demonstrated utility in the following weather situations:

- Diagnosing a sea-breeze passage at the SLF.

- Depicting high-resolution quantitative characteristics of cloud fields such as ceilings, cloud-top heights, cloud liquid content, cloud ice content, etc.

- Monitoring the magnitude of cross, head, and/or tailwind components at the SLF.

- Assessing stability indices (CAPE, Lifted Index, Microburst Day Potential Index, etc.) at high temporal and spatial resolutions to determine thunderstorm risks.

LDIS provided an integrated product which was valuable in diagnosing several different weather events within a two-week period during the Florida cool-season. The weather features and boundary interactions during the cool season are typically far less complex than warm-season phenomena. Therefore, the potential utility of a real-time LDIS during the Florida warm-season is likely substantial considering the valuable results demonstrated during the cool-season simulation.

8.4 Summary of LDIS Sensitivities / Deficiencies

Several system sensitivities and deficiencies related to available real-time data were presented in Section 6. A comparison between the influence of level II versus level III WSR-88D data on subsequent ADAS analyses was conducted for a 9-h period on 28 February during a pre-frontal thunderstorm event in east-central Florida. The results from this experiment revealed the following comparisons between using the full volume level II versus level III data.

- In general, the number of remapped radial velocity observations on the 2-km analysis grid using level II data greatly exceeds the number of remapped radial velocity observations using level III data.

- A consequence of the increased number of radial velocity observations associated with level II data is the ability to detect more efficiently subtle boundaries and wind shift lines such as the low-level cold front on 28 February. A band of convergence associated with the low-level cold front was depicted in the analyses using level II data but was not detected by analyses using level III data.

- The benefits of using level II WSR-88D data can be even more important during the Florida warm season when boundary interactions are most numerous.

- Despite the greater volume of level II versus level III WSR-88D data, the analyzed cloud and moisture fields using level II data are similar to the analyzed cloud and moisture fields using level III data.

- The analyzed vertical velocity fields are much stronger in magnitude and can depict more fine-scale circulations using level II data rather than level III data.

- A significant benefit gained by ingesting level III data from all Florida radar sites is the nearly continuous horizontal coverage of radar data at low levels.

Additional system sensitivities occurred as a result of missing or deficient GOES-8 satellite data and missing RUC background fields. These sensitivities are summarized as follows.

- The analyzed cloud variables are deficient during fixed synoptic times when SMG does not receive GOES-8 infrared (IR) and visible (VIS) data. When no GOES-8 data are available and WSR-88D reflectivity data do not contribute significantly, METAR cloud observations are the primary data source contributing to the cloud analysis.

- Albedo data derived from GOES-8 VIS imagery become unreliable during sunrise and sunset due to the low sun angle. These albedo data are discarded when the sun angle drops below a threshold angle. A sharp transition in the ADAS-derived cloud fields can occur within successive analyses when VIS data are no longer used in the complex cloud scheme of ADAS.

- The analysis cycle requires a background field from a large scale model such as the Rapid Update Cycle (RUC) model. RUC 3- and 6-h forecasts were used as background fields for the 10-km ADAS analyses. During certain three-hour intervals when RUC forecasts were missing from the data archive, ADAS analyses could not be generated. This problem could be amended by using an older RUC forecast or an Eta forecast grid as a background field for the 10-km ADAS analyses.

8.5 Towards a Real-time Implementation of LDIS

This final section addresses the remaining issues that are necessary in order to install and implement LDIS at SMG, NWS MLB, or 45 WS. These issues include additional required software used by the AMU in the current configuration, wall-clock time considerations for data ingest programs and graphical post-processing, the advantages and disadvantages associated with installing the latest version of ARPS/ADAS, and the hardware platform on which to run LDIS.

8.5.1   Software Used in this Task

During the course of this task, the AMU extensively utilized two software packages for data conversion and graphical post-processing. McIDAS-X version 7.501 was used for most of the data pre-processing programs that involved text or point data (e.g. surface data, KSC/CCAS data, rawinsondes, etc.). GEMPAK software version 5.4 was utilized for the generation of all routine graphics and NTRANS was used to examine the routine products that were produced. NTRANS reads GEMPAK-generated files and consists of a graphical user interface with animation capabilities that can be used to examine multi-panel imagery.

In order to realize the smoothest transition during the installation of LDIS, the AMU recommends that the following additional software be installed prior to an LDIS installation.

- McIDAS-X version 7.5 or higher with the ADDE capability to run data ingestors for MIDDS data.

- GEMPAK version 5.4 or higher with the NTRANS graphical user interface for post-processing of LDIS analyses.

8.5.2   Additional Real-time Issues

The following issues related to wall-clock time also need to be addressed when considering the installation of a real-time LDIS.

- All data ingestors need to be reconfigured to process each individual data set as soon as the data are received in real-time.

- Additional wall clock time for each analysis cycle is required to remap WSR-88D and GOES-8 data. These data ingestor routines require the most wall-clock time to run compared with all other data sources (a few minutes collectively for all six Florida radar sites, GOES-8 IR, and GOES-8 VIS imagery).

- Wall-clock time for graphics generation varies considerably depending on the complexity and total number of plots generated. Images with a substantial amount of color shading, filtering, and diagnostic computations take considerably longer to plot than simple contoured images.

8.5.3   Latest Version of ADAS

If AMU customers choose to install ADAS as configured by the AMU, it may be advantageous to obtain the latest version of ARPS/ADAS from the University of Oklahoma rather than the AMU's version used in LDIS Phases I and II. The reasons for this recommendation are as follows.

- Better technical support could be provided from the ARPS/ADAS developers by using the latest available version of ARPS/ADAS.

- The latest version will include the most recent code improvements and fixes.

- If experiments were conducted with ARPS, it would be advantageous to use the most recent version of the model that contains several improvements and additional features not available with the older version of ARPS/ADAS used by the AMU. However, AMU customers could have the option of running the ARPS numerical prediction model in conjunction with ADAS *regardless of the version chosen*.

The primary disadvantage in upgrading to the latest version of ARPS/ADAS is that it will require a higher level of effort to install and configure the software. The code developed and modified by the AMU during LDIS Phases I and II would have to be carefully incorporated into the latest version of the ARPS/ADAS code prior to configuring the system. The modifications would primarily involve the incorporation of data ingestors designed specifically for KSC/CCAS observations.

8.5.4   Hardware Platform

Another important decision for implementing a real-time LDIS is the hardware selection. ARPS/ADAS personnel have benchmarked their software on the following hardware platforms: IBM RS/6000, Cray, Connection Machine CM-200 and CM-5, DEC ALPHA 3000 Model 800, Sun SPARCstation 10 Model 51, SGI Power Challenge XL, among others (Xue et al. 1995). However, both SMG and NWS MLB currently have HP platforms which could be used for installing LDIS. ARPS/ADAS has not been tested extensively on HP hardware and would likely require a benchmark test to prove its fidelity on an HP workstation.

9.0 References

Albers, S. C., J. A. McGinley, D. A. Birkenheuer, and J. R. Smart, 1996: The local analysis and prediction system (LAPS): Analysis of clouds, precipitation, and temperature. *Wea. Forecasting*, **11**, 273-287.

Anthes, R. A., 1983: Regional models of the atmosphere in middle latitudes. *Mon. Wea. Rev.*, **111**, 1306-1335.

Benjamin, S. G., J. M. Brown, K. J. Brundage, D. Devenyi, B. E. Schwartz, T. G. Smirnova, T. L. Smith, L. L. Morone, and G. J. DiMego, 1998: The operational RUC-2. *16th Conf. on Weather Analysis and Forecasting*, Phoenix, AZ, Amer. Meteor. Soc., 249-252.

Benjamin, S., and K. Brundage, FSL, cited 1999: MAPS/RUC Information. [Available on-line from http://maps.fls.noaa.gov.]

Bergthorsson, P., and B. Doos, 1955: Numerical weather map analysis. *Tellus*, **7**, 329-340.

Bratseth, A., 1986: Statistical interpolation by means of successive corrections. *Tellus*, **38A**, 439-447.

Brewster, K., 1996: Application of a Bratseth analysis scheme including Doppler radar data. Preprints, *15th Conf. on Weather Analysis and Forecasting*, Norfolk, VA, Amer. Meteor. Soc., 92-95.

Case, J. L., and J. Manobianco, 1998: Final report on prototype local data integration system and central Florida data deficiency. NASA Contractor Report CR-1998-208540, Kennedy Space Center, FL, 57 pp. [Available from ENSCO, Inc., 1980 N. Atlantic Ave., Suite 230, Cocoa Beach, FL 32931].

Cole, R. E., and W. W. Wilson, 1995: ITWS gridded winds product. Preprints, *6th Conf. on Aviation Weather Systems*, Dallas, TX, Amer. Meteor. Soc., 384-388.

Gray, D. G., C. M. Hayden, and W. P. Menzel, 1996: Review of quantitative satellite products derived from GOES-8/9 imager and sounder instrument data. Preprints, *8th Conf. on Satellite Meteor. and Oceano.*, Atlanta, GA, Amer. Meteor. Soc., 159-163.

McPherson, R., 1999: The future of the North American radiosonde network. Preprints, *3rd Symp. on Integrated Observing Systems*, Dallas, TX, Amer. Meteor. Soc., 14-17.

Neiman, S. J., W. P. Menzel, C. M. Hayden, D. Gray, S. T. Wanzong, C. S. Veldon, and J. Daniels, 1997: Fully automated cloud-drift winds in NESDIS operations. *Bull. Amer. Meteor. Soc.*, **78**, 1121-1133.

Schwartz, B., and S. G. Benjamin, 1995: A comparison of temperature and wind measurements from ACARS-equipped aircraft and rawinsondes. *Wea. Forecasting*, **10**, 528-544.

Snook, J. S., P. A. Stamus, and J. Edwards, 1998: Local-domain analysis and forecast model support for the 1996 Centennial Olympic Games. *Wea. Forecasting*, **13**, 138-150.

Veldon, C. S., C. M. Hayden, S. J. Nieman, W. P. Menzel, S. Wanzong, and J. S. Goerss, 1997: Upper-tropospheric winds derived from geostationary satellite water vapor observations. *Bull. Amer. Meteor. Soc.*, **78**, 173-195.

Xue, M., K. K. Droegemeier, V. Wong, A. Shapiro, and K. Brewster, 1995: ARPS version 4.0 user's guide. 380 pp. [Available from the Center for Analysis and Prediction of Storms, University of Oklahoma, Norman, OK, 73019-1011.]

Zhang, J., F. H. Carr, and K. Brewster, 1998: ADAS cloud analysis. Preprints, *12th Conf. on Numerical Weather Prediction*, Phoenix, AZ, Amer. Meteor. Soc., 185-188.

Appendix

ADAS Complex Cloud Scheme

The ADAS complex cloud scheme (CCS, Zhang et al. 1998) is based on the cloud analysis algorithms of the Local Analysis and Prediction System (LAPS, Albers et al. 1996) and includes some modifications. The CCS was designed to provide detailed initial conditions for moisture variables in the Advanced Regional Prediction System (ARPS) numerical weather prediction model (Xue et al. 1995). The CCS algorithm consists of a four-step process for empirically constructing and fine-tuning analyzed cloud fields. First, cloud reports from Aviation Routine Weather Report (METAR) stations are ingested to provide information about cloud bases. Second, GOES-8 infrared (IR) imagery are used to construct the cloud-top heights. WSR-88D reflectivity data are used in the third step to provide a three-dimensional representation of the cloud fields. Finally, GOES-8 visible (VIS) data are used to remove areas of excess cloud cover. Each of these steps of the CCS are discussed in more detail below and are found in Zhang et al. (1998).

1. METAR Cloud Reports

Surface-based cloud observations provide the CCS of ADAS with information on cloud bases and the heights of multiple cloud layers. METAR cloud reports (clear, scattered, broken, or overcast with accompanying cloud base heights) are inserted onto the ADAS analysis grid with a prescribed horizontal influence radius and thickness. The influence radius prevents an overestimate of the areal coverage of the analyzed clouds. An assumed thickness of about 1 km is applied above the reported cloud base heights.

2. GOES-8 IR data

The 4-km resolution GOES-8 IR imagery consists of brightness temperature data that are compared to the existing ADAS gridded temperature field and METAR cloud analysis. Addition (reduction) of analyzed clouds are performed on grid points in which the observed satellite brightness temperatures are colder (warmer) than the expected ADAS brightness temperatures. When a high-cloud layer is added, an assumed thickness of 1.5 km is applied. The cloud is positioned such that the satellite brightness temperature matches the existing ADAS analyzed temperature field. Details on the brightness temperature thresholds and a description of how the algorithm handles low cloud cover are found in Albers et al. (1996).

3. WSR-88D data

After the WSR-88D reflectivity data are remapped and assigned to specific grid points in the ADAS domain, cloud variables are analyzed based on assigned reflectivity thresholds. When a grid point is influenced by multiple radars, the maximum reflectivity is used for the cloud analysis. Reflectivity data are interpolated between radar beams to form a continuous volume of observations. Reflectivity thresholds are used for quality control to remove features such as ground clutter. The reflectivity data provide the best means for a nearly continuous three-dimensional cloud field on the ADAS analysis grid.

4. GOES-8 VIS data

In order to fine-tune the analyzed cloud variables from steps 1-3, a cloud albedo field is derived from the 1-km GOES-8 VIS imagery. The total cloud field from the albedo data and the existing ADAS cloud analysis are compared. The ADAS-analyzed cloud fields are removed in areas where it exceeds the total cloud cover derived from the albedo data.

NOTICE